Effective interactions for the $0p1s0d$ nuclear shell-model space

E. K. Warburton
Brookhaven National Laboratory, Upton, New York 11973

B. A. Brown
National Superconducting Cyclotron Laboratory and Department of Physics and Astronomy, East Lansing, Michigan 48824

(Received 17 April 1992)

Shell-model interactions are constructed in the cross-shell model space connecting the $0p$ and $1s0d$ shells with due regard for the perturbative effects of the neighboring $0s$ and $0f1p$ shells. The interactions have three distinctive $0p$-shell, cross-shell, and $1s0d$-shell parts. The latter is taken to be the previously determined W interaction. The $0p$-shell interaction is represented by two-body matrix elements and the cross-shell by either a potential or by two-body matrix elements. The interactions are determined by least-squares fits to 51 $0p$-shell and 165 cross-shell binding energies. It is found that the addition of monopole terms to a potential that is otherwise similar to that of the Millener-Kurath interaction results in a great improvement in the fit. In the fit to two-body matrix elements, 45 of 97 possible linear combinations of parameters are varied and the root-mean-square deviation for the 165 cross-shell energies is 330 keV. Examples of the application of the interactions are given for the prediction of neutron-rich binding energies, Gamow-Teller decays, and $0\hbar\omega$, $1\hbar\omega$, and $2\hbar\omega$ energy spectra.

PACS number(s): 21.60.Cs, 27.20.+n, 21.10.Dr, 23.40.Hc

I. INTRODUCTION

Much progress has been made in recent years on our understanding of nuclear states which, to a good approximation, have all active nucleons in a single one of the first four major shells, i..e., $0s$, $0p$, $1s0d$, and $0f1p$. Most notable has been the great success of effective interactions obtained by least-squares fitting experimental binding energies to single-particle energies (SPE) and either two-body matrix elements (TBME) or the parameters of a potential. The classic fit to the $0p$ shell which illustrated the power of this method was made by Cohen and Kurath [1] in 1965. Results for the $1s0d$ shell were obtained by Wildenthal and colleagues [2–6]. In the earlier of these studies, the interaction was mass independent and separate fits were made to the lower and upper half of the $1s0d$ shell. An important advance made by Wildenthal [4] in building the W interaction [6] was to scale the TBME as $(A/18)^{-p_A}$ with p_A=0.3. With this assumption it was finally possible to obtain a good fit to the entire $1s0d$ shell. Subsequently it has been found that the $0p$ shell fit—originally made [1] with mass-independent SPE—is better if the interaction is assumed to scale as $(A/16)^{-0.17}$ [7]. The number of TBME for the $0p$ shell and $1s0d$ interactions are 15 and 63. These numbers are small enough compared to the body of experimental data so that a least-squares fit can be made with the TBME as variables. However the TBME are not all well determined since some do not have a strong dependence on the low-lying level energies. Thus, an important advance in the $1s0d$ study of Chung and Wildenthal [3] was the utilization of the linear combination (LC) method—also termed the direct combination method (DCM) [8]—in which the error matrix representing the relationship of the TBME to the level energies is diagonalized, thus giving linear combinations which are independent of each other [3, 5, 8]. Then only those linear combinations of parameters which are well determined (by some external criterion) are varied, the remaining being frozen at some "background" value. The method of least-squares fitting with TBME and SPE as parameters was termed the model-independent (MI) method by Brown, Richter, Julies, and Wildenthal [5], hereafter referred to as BRJW. Here we have described the MI-LC method.

There are two criteria which can be used to judge these empirical $0p$ and $1s0d$ interactions. First, are the resulting wave functions realistic so that other observables can be predicted reliably? Second, are the empirical interactions in satisfactory agreement with our fundamental understanding of nuclei and the nucleon-nucleon interaction? These empirical interactions meet both criteria with astonishing success. An example of the predictive power for other observables is the study of M1 and Gamow-Teller observables in the $1s0d$ shell by Brown and Wildenthal [6, 9]. As for the second criteria, the TBME of the Cohen-Kurath and W interactions are in remarkably good agreement [5] with the "bare G-matrix plus core-polarization" TBME obtained by the Kuo-Brown method [10, 11]. It is these Kuo-Brown TBME that Wildenthal used for "background" in his application of the MI-LC method in obtaining the W interaction.

For the major shells above mass 40 it is more difficult to make a least-squares fit with the TBME and SPE as parameters because of the larger number of TBME (195 for the $0f1p$ shell) and a lack of sufficient data. A practical alternative is to represent the interaction by a

potential and vary its parameters. This will result in a more and more constrained fit as the dimensions of the model space increase. In the $0p$ shell the 15 TBME can be formally replaced by a 15-parameter two-body LS potential so that fitting to the TBME or to this potential gives identical results [1]. But in higher shells the use of a potential with a limited number of parameters offers an attractive alternative to the MI-LC method of constraint. We refer to the use of a potential as the model-dependent (MD) method. The use of a one-boson-exchange potential (OBEP) plus core-polarization correction terms of the multipole-multipole type to describe $1s0d$ nuclei was exhaustively studied by BRJW. The method has been applied to the $0f1p$ [12] and $0p$ [7] shells. These results illustrate the power of the method.

There has been less progress in our understanding of cross-shell states in these nuclei; i.e., states which have active nucleons in more than one major shell. Important steps in our understanding of these states are the classic particle-hole calculations of Elliot and Flowers [13] for ^{16}O and of Halbert and French [14] for ^{15}N. These calculations used a schematic central particle-hole interaction. They demonstrated that the low-lying non-normal parity states of these nuclei were well described by a $1\hbar\omega$ excitation of the $(0s_{1/2})^4(0p)^{A-4}$ configuration. Calculations of this type culminated in the successful and oft-used Millener-Kurath (MK) interaction connecting the $0p$ and $1s0d$ shells [15]. The 80 $1\hbar\omega$ "cross-shell" TBME of this interaction were generated from a potential (OBEP) containing central, tensor and spin-orbit terms with a single Yukawa radial form for each. The form of the potential and the strengths of the various terms were carefully chosen from consideration of previous studies — such as those of Refs. [13,14] — and of excitation energies of non-normal parity states in A=15 and 16 nuclei, and from a desire to stay close to the form and strength of Kuo's bare G-matrix potential [10]. When used in conjunction with the Cohen-Kurath $0p$-shell interaction [1] and the W interaction [4] — or one of its precursors [2, 3] — the MK interaction has given us a quite successful description of $2\hbar\omega$ and $3\hbar\omega$ states in A=10–22 nuclei as well as the $1\hbar\omega$ states for which it was originally designed. This success implies the weak-coupling of the $0p$ and $1s0d$ shells which, in fact, was anticipated by the very simple calculations of Talmi and Unna [16]. Indeed shell-model calculations explicitly formulated as weak-coupling of these major shells have given very successful descriptions of nuclei near ^{16}O. In particular we note the elegant formulation of Ellis and Engeland [17] and the many successful calculations made with it [18–21]. The weak-coupling approach of Ellis and Engeland has attractive features, the most notable being the sizable reduction in the dimensions of the diagonalizations. The weak-coupling approach is probably the most practical for cross-shell calculations above the $0f1p$ shell, but with present-day computer resources this reduction is not an important consideration for the lighter nuclei.

The most notable studies of cross-shell states near ^{16}O since the MK interaction have been those of the Utrecht group [22–27]. These use a quite different approach than those outlined here. A comparison to the present results will be made at the end of this article.

The original motivation for the present study was the desire for an effective cross-shell interaction for the $0p1s0d$ shells of the MK type but with a more complex cross-shell potential with more quantitatively determined parameters and therefore, hopefully, more accurate wave functions. As this study progressed it became clear that an equally accurate and physically meaningful interaction could be obtained by the MI-LC method. Construction of both types of interactions will be described. The bulk of the computations described herein were carried out with the shell-model code OXBASH [28]. With Oxbash, spurious center-of-mass motion is removed by the usual method [29] of adding a center-of-mass Hamiltonian $H_{\rm c.m.}$ to the interaction.

Anticipated uses of the interactions include, e.g., binding energies and Gamow-Teller β decay rates for neutron-rich nuclei, first-forbidden β decay observables [30], and parity nonconservation [31, 32]. Examples of the calculation of such observables will also be described. Any of the interactions discussed in this article are available by regular or electronic mail upon request to one of the authors.

In the next section we present a brief table of definitions used in this study. The data selection is discussed in Sec. III, and the potentials and the least-squares fits are described in Sec. IV. Results are discussed in Secs. V and VI.

II. NOMENCLATURE

The present study is complex enough so that some difficulty may be encountered in following the unavoidable definitions and acronyms. To aid in this task we have tabulated in Table I in alphabetical order some of the more often used or potentially confusing of these quantities.

III. THE BINDING ENERGY DATA

A. Coulomb corrections

The shell-model interactions used in this study contain no Coulomb terms. In our procedure the Coulomb plus core contribution to the total experimental binding energy $E_{B_{\rm exp}}$ is estimated and subtracted off to yield the experimental datum $E_{B_{\rm corr}}$ used in the fits. As discussed by Brussard and Glaudemans [8], there are several ways to estimate the Coulomb energies. Our procedure is the same as that of Cohen and Kurath [1] in their $0p$-shell study, and Chung and Wildenthal [3] and later Wildenthal [4] in their $1s0d$-shell studies; namely, within the valley of stability, the Coulomb energy for given Z is taken to be independent of A. The error due to this assumption is minimized by the method of referring all energies to the valley of stability [$T_z = (N-Z)/2 = 0$ or $+\frac{1}{2} \equiv T_{z_{\rm min}}$] by the use of analogue states. When venturing far enough from the valley of stability so that the analogue of the T_z state is not known in the $T_z - 1$ nucleus, the mass-independent assumption is dropped and

the excitation energy of the analogue of T_z in the $T_{z_{\min}}$ nucleus is estimated using mass-dependent Coulomb displacement energies. Thus (a) the use in the fits of experimental masses of off-stability nuclei and (b) the reverse procedure, namely, the predictions of the masses of such nuclei not included in the fits, is to be supplemented by an estimate of the mass dependence of the Coulomb energies. This aspect of the predictions is discussed further in Sec. VI A.

Our bench mark for the Coulomb-corrected binding energy $E_{B_{\rm corr}}$ is that of ^{16}O which, following Cohen and Kurath, we take as -113.157 MeV relative to ^{4}He. Then $E_{B_{\rm corr}}(^{14}{\rm O})$, e.g., is obtained from the experimental binding energies of ^{16}O and ^{14}O via

$$E_{B_{\rm corr}}(^{14}{\rm O}) = -113.157 - [E_{B_{\rm exp}}(^{16}{\rm O}) - E_{B_{\rm exp}}(^{14}{\rm O})] = -84.271 \text{ MeV}, \quad (1)$$

and $E_{B_{\rm corr}}(^{14}{\rm N})$ is given by $E_{B_{\rm corr}}(^{14}{\rm O})-2.313$ MeV. The $E_{B_{\rm corr}}$ for the A=12–14 nuclei are then obtained from $E_{B_{\rm corr}}(^{14}{\rm C})\equiv E_{B_{\rm corr}}(^{14}{\rm O})$, the differences in the $E_{B_{\rm exp}}$ values for the carbon isotopes, and from analogue-state energies; while the A=10–11 $E_{B_{\rm corr}}$ values are obtained in a similar manner from the B isotopes. The flow chart of Fig. 1 illustrates the procedure used which results in the

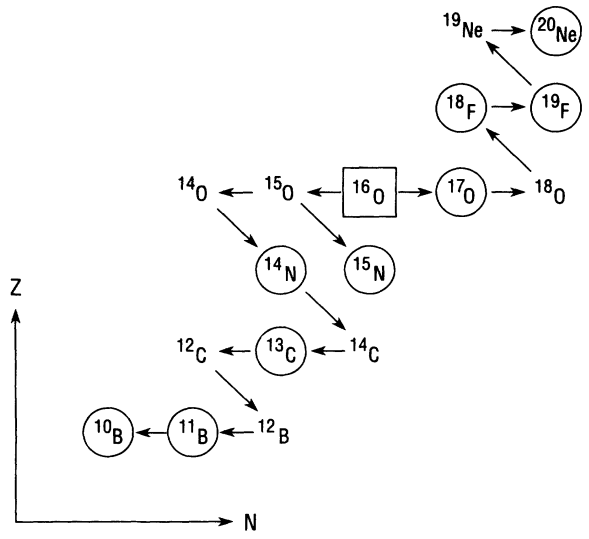

FIG. 1. Flow chart illustrating the route taken in evaluating the $E_{B_{\rm corr}}$ of A=10–20 nuclei relative to ^{16}O. Horizontal arrows assume mass-independent Coulomb energies, forty-five degree arrows assume the equality (apart from the Coulomb energy) of analogue states. Reference nuclei (T_z=0 or $\frac{1}{2}$) are circled.

TABLE I. Nomenclature.

BRJW	The $1s0d$-shell study of Brown, Richter, Julies, and Wildenthal [5].
$E_{B_{\rm exp}}$	Experimental binding energy (a negative quantity).
$E_{B_{\rm corr}}$	$E_{B_{\rm exp}}$ with the Coulomb energy subtracted.
Δ_{sfp}	A correction to the psd values of $E_{B_{\rm corr}}$ for the influence of the $0s$ and $0f1p$ shells.
HKT	The one-boson-exchange potential of Hosaka, Kubo, and Toki [33].
LC	The linear combination method of least-squares fitting.
MD	Model-dependent fit to a potential plus SPE.
MI	Model-independent fit to TBME plus SPE.
MK	The Millener-Kurath *psd* interaction.
$\mathcal{N}$	The principal quantum number of the oscillator (= 0,1,2...).
OBEP	One-boson-exchange potential.
OPEP	One-pion-exchange potential.
PKUO	The Kuo interaction based on the Paris nucleon-nucleon interaction; the SPE were determined by a least-squares fit to A=10–16 levels.
POT($n_p, n_{\rm spe}, p_A$)	An n_p parameter potential plus $n_{\rm spe}$ SPE parameters and an A dependence of the TBME characterized by $(16/A)^{p_A}$.
P(10–16)T	The MI fit to the 51 A=10–16 energy levels of Table III.
P(5–16)T	The MI fit to 86 A=5–16 energy levels.
PSDP	The psd fit with TBME for the p shell and POT(10,2,0.0) for the cross shell.
PSDT	The 45-variable MI-LC psd fit.
PWBP	p-shell part of the psd fit PSDP with TBME for the p shell and POT(10,2,0.0) for the cross shell.
PWBT	p-shell part of the 45-parameter MI-LC psd fit PSDT.
Q	The number of quanta in a major oscillator shell (= $2\mathcal{N} + l$), where l is the orbital angular momentum.
SPE	Single-particle energy.
TBME	Two-body matrix element.
W	The $1s0d$ interaction of Wildenthal.
WBP	The *spsdpf* interaction based on the psd PWBP interaction.
WBT	The *spsdpf* interaction based on the psd PWBT interaction.

$E_{B_{\rm corr}}$ of Table II. Note that there are usually several possible routes from one nucleus to another; our procedure is not unique. The different routes give $E_{B_{\rm corr}}$ values which differ by $\lesssim$150 keV. An example would be the evaluation for ^{14}N:

route 1: ^{16}O→^{15}O→^{14}O→^{14}N=−86.584 MeV,

route 2: ^{16}O→^{15}O→^{15}N→^{14}N=−86.659 MeV.

These differ by 75 keV.

The $E_{B_{\rm corr}}$ for A=17–22 nuclei (relative to that for ^{16}O) are taken from the work of Chung and Wildenthal [3, 4, 34]. The E_c for A=5–9 are from Cohen and Kurath [1]. The $E_{B_{\rm corr}}$ for most other A=5–22 isotopes can be obtained from those of Table II using analogue-state energies in the T_z=0 and $+\frac{1}{2}$ isotopes. The exceptions are discussed in Sec. VI A.

B. General considerations

A word about nomenclature: There is some ambiguity in the literature as to the meaning of $n\hbar\omega$ states (n=0,1,2...) and $n\hbar\omega$ excitations. For given A we refer excitation energies to the T_z=0 or $+\frac{1}{2}$ nucleus and define the ground-state (lowest allowed by the Pauli principal) configuration as $0\hbar\omega$. Then states which — in our *psd* model space — are composed of a $0p \rightarrow 1s0d$ ($\Delta T \leq 1$) one particle-one hole (1p-1h) excitation of this configuration are labeled $1\hbar\omega$, 2p-2h ($\Delta T \leq 2$) excitations give $2\hbar\omega$ states, etc.

TABLE II. Coulomb-corrected binding energies $E_{B_{\rm corr}}=E_{B_{\rm exp}}-E_c$+28.296 MeV for A=5–22 nuclei. E_c is the Coulomb energy at the valley of stability (with the Coulomb energy of ^{4}He subtracted) and −28.296 MeV is $E_{B_{\rm exp}}$ for ^{4}He. Note that the A dependence of E_c for neighboring isotopes in the valley of stability is neglected. The E_c for the first five entries are from Ref. [1] and the $E_{B_{\rm corr}}$ for $A > 16$ are from Ref. [3].

Nucleus	$E_{B_{\rm exp}}$ (MeV)	E_c (MeV)	$E_{B_{\rm corr}}$ (MeV)
^{5}He	− 27.410	0.000	+ 0.886
^{6}Li	− 31.996	1.000	− 4.700
^{7}Li	− 39.246	1.000	− 11.950
^{8}Be	− 58.165	2.640	− 30.844
^{9}Be	− 56.500	2.640	− 32.509
^{10}B	− 64.751	4.751	− 41.206
^{11}B	− 76.205	4.751	− 52.660
^{12}C	− 92.162	7.282	− 71.148
^{13}C	− 97.109	7.282	− 76.095
^{14}N	−104.659	10.221	− 86.584
^{15}N	−115.493	10.296	− 97.493
^{16}O	−127.620	13.833	−113.157
^{17}O	−131.764	13.833	−117.301
^{18}F	−137.370	17.313	−126.387
^{19}F	−147.802	17.334	−136.840
^{20}Ne	−160.650	21.282	−153.636
^{21}Ne	−167.411	21.282	−160.396
^{22}Na	−174.149	25.563	−171.416

Experimental excitation energies are mainly from the compilations of Ajzenberg-Selove [35]. Unless explicitly noted, we follow all Ajzenberg-Selove's adopted (J^π, T) assignments including those not considered definite (as denoted by parentheses in Ref. [35]). We will explain the origin of the remainder of the E_x and the reason for some of the less obvious choices of data. One of the most powerful tools for distinguishing between $0\hbar\omega$ and $\geq 2\hbar\omega$ levels is via reactions involving the pickup of one or more particles. The cross sections to $0\hbar\omega$ states are expected — and found — to be large compared to those to $\geq 2\hbar\omega$ states. In contrast, stripping reactions such as, e.g., ^{10}B(^{6}Li,^{3}He)^{13}C, will not distinguish between these groups of states and often will accentuate $2\hbar\omega$ states. An example of the use of such data in the identification of the $0\hbar\omega$ states of ^{13}C is discussed by Millener *et al.* [36] in a study of the ^{13}C$(e,e')^{13}$C reaction. For brevity and clarity we refer to a level by the index given in the first column of the tables which follow.

It is convenient to give the $E_{B_{\rm corr}}$ for all states of a fixed A value as an excitation energy in the T_z=0 or $+\frac{1}{2}$ nucleus of the same A. We stress that the extraction of a mass prediction for a $T_z > T_{z_{\rm min}}$ member of the $2T_z + 1$ multiplet may involve the use of mass-dependent Coulomb displacement energies as explained in Sec. VI A. Unless otherwise noted, excitation energies are taken from the most neutron-rich nucleus available with the ground-state energy relative to the T_z=0 or $\frac{1}{2}$ nucleus given as discussed above. Model states are identified by (J^π_k, T) where k orders the model states of a particular (J^π, T) in energy. When no confusion should arise (between states belonging to different configurations), experimental states are also so designated.

C. The 0*p*-shell data

In the 0*p*-shell fits to the A=5–16 region, 35 levels in the A=5–9 region were used together with the 51 levels of Table III. These 35 levels are the 34 listed by Julies *et al.* [7] together with the second 2^+, T=0 level of ^{8}Be taken to lie at the same energy as the first 2^+, T=1 level with the isospin mixing between them turned off, i.e., for both the $(2^+_2, 0)$ and $(2^+_1, 1)$ states we take E_x=(16626+16922)/2=16774 keV.

The selection of the A=10–16 0*p*-shell data is self-explanatory with these few exceptions.

^{14}N. The excitation energies of Nos. 7 and 8 are C^2S-weighted centroid energies calculated from the ^{15}N(p,d)^{14}N C^2S results of Saha *et al.* [37]. It is well-known that the ^{14}C 2^+ states at 7.012 and 8.318 MeV (or the ^{14}N 2^+ states at 9.171 and 10.434 MeV) are approximately equal mixtures of the $(2^+, 1)$ states of the $0\hbar\omega$ and $2\hbar\omega$ configurations [38]. We assume the state observed by Saha *et al.* at 12505 keV is the third $(2^+, 1)$ state of ^{14}N [thus supplying the needed analogue of the ^{14}C $(2^+, 1)$ 10425-keV level] rather than the third $(1^+, 0)$ state that they suggest. Then, the E_x listed for No. 8 is the C^2S-weighted centroid for the lowest three $(2^+, 1)$ states.

^{13}C. The selection of the ^{13}C $0\hbar\omega$ states was aided by

TABLE III. The A=10–16 p-shell states included in the p-shell and cross-shell fits. The last two columns are results for the PWBT interaction. The last column is experiment (Expt.) − theory for E_x.

No.	Nucleus	$2J^\pi$	$2T$	k	E_x (MeV) Expt.	Theory	Δ
1	^{16}O	0^+	0	1	0.000	− 0.499	0.499
2	^{15}N	1^-	1	1	0.000	− 0.195	0.195
3	^{15}N	3^-	1	1	6.324	6.279	0.045
4	^{14}N	2^+	0	1	0.000	0.013	−0.013
5	^{14}N	0^+	2	1	2.313	2.486	−0.173
6	^{14}N	2^+	0	2	3.948	4.010	−0.062
7	^{14}N	4^+	0	1	7.190	7.081	0.109
8	^{14}N	4^+	2	1	10.149	10.212	−0.063
9	^{14}N	6^+	0	1	11.050	11.321	−0.271
10	^{14}N	2^+	2	1	13.619	13.156	0.463
11	^{13}C	1^-	1	1	0.000	− 0.059	0.059
12	^{13}C	3^-	1	1	3.685	4.351	−0.666
13	^{13}C	5^-	1	1	7.547	7.934	−0.387
14	^{13}C	1^-	1	2	8.860	9.233	−0.373
15	^{13}C	3^-	1	2	11.748	11.329	0.419
16	^{13}C	7^-	1	1	12.438	12.634	−0.196
17	^{13}C	3^-	3	1	15.108	15.139	−0.031
18	^{13}C	1^-	3	1	18.732	19.574	−0.842
19	^{12}C	0^+	0	1	0.000	− 0.363	0.363
20	^{12}C	4^+	0	1	4.439	4.885	−0.446
21	^{12}C	0^+	0	2	10.300	10.114	0.186
22	^{12}C	2^+	0	1	12.710	13.132	−0.422
23	^{12}C	8^+	0	1	14.083	14.276	−0.193
24	^{12}C	2^+	2	1	15.110	15.155	−0.045
25	^{12}C	4^+	2	1	16.063	16.018	0.045
26	^{12}C	0^+	2	1	17.833	17.840	−0.007
27	^{12}C	4^+	2	2	18.869	19.104	−0.235
28	^{12}C	2^+	2	2	20.110	19.751	0.359
29	^{12}C	6^+	2	1	20.722	20.275	0.447
30	^{12}C	0^+	4	1	27.860	28.388	−0.528
31	^{11}B	3^-	1	1	0.000	− 0.263	0.263
32	^{11}B	1^-	1	1	2.125	1.721	0.404
33	^{11}B	5^-	1	1	4.445	4.293	0.152
34	^{11}B	3^-	1	2	5.020	5.007	0.013
35	^{11}B	7^-	1	1	6.743	6.424	0.319
36	^{11}B	5^-	1	2	8.920	8.751	0.169
37	^{11}B	1^-	3	1	12.916	13.024	−0.108
38	^{11}B	9^-	1	1	13.137	12.975	0.162
39	^{11}B	3^-	5	1	33.950	33.506	0.444
40	^{10}B	6^+	0	1	0.000	0.468	−0.468
41	^{10}B	2^+	0	1	0.718	0.922	−0.204
42	^{10}B	0^+	2	1	1.740	1.348	0.392
43	^{10}B	2^+	0	2	2.154	2.713	−0.559
44	^{10}B	4^+	0	1	3.587	3.452	0.135
45	^{10}B	6^+	0	2	4.774	4.982	−0.208
46	^{10}B	4^+	2	1	5.108	5.343	−0.235
47	^{10}B	4^+	0	2	5.920	5.305	0.615
48	^{10}B	8^+	0	1	6.025	5.999	0.026
49	^{10}B	2^+	0	3	7.467	7.382	0.085
50	^{10}B	4^+	2	2	7.698	7.328	0.370
51	^{10}B	8^+	2	1	13.572	13.399	0.173

the (e,e') results of Ref. [36] as well as the ^{16}O$(p,\alpha)^{13}$N, ^{15}N$(p,^3$He$)^{13}$C, and ^{15}N$(p,t)^{13}$N results of Maples and colleagues [39]. The two lowest-lying $0\hbar\omega$ states of ^{13}B are predicted with any of the available $0p$-shell interactions to be the $\frac{3}{2}^-$ ground state and a $\frac{1}{2}^-$ excited state some 2–5 MeV higher. The two experimental candidates for the $\frac{1}{2}^-$ state are at E_x=3536 and 3712 keV. These states are close enough so that we can use the mean energy of 3624 keV for No. 18 without introducing appreciable error.

^{12}C. All even-parity T=0 levels (Nos. 19–23) below 16 MeV in ^{16}O are included except the 0^+ 7654-keV level and the possible 2^+ 11160-keV level, both of which we assume to be $\geq 2\hbar\omega$ states. All T=1 levels with $E_x(^{12}\text{B})<6$ MeV are included.

^{11}B. All odd-parity states below 10 MeV are included except the third $\frac{3}{2}^-$ state at 8560 keV. Also included are the yrast $(\frac{9}{2}^-,\frac{1}{2})$ and $(\frac{1}{2}^-,\frac{3}{2})$ states.

^{10}B. All even-parity T=0 states with $E_x(^{10}\text{B})<7.5$ MeV are included except the $2\hbar\omega$ 5180-keV $(1^+,0)$ state [40] and the 7002-keV level. All T=1 states with $E_x(^{10}\text{Be})<8.0$ MeV are included except the $2\hbar\omega$ 6179-keV $(0^+,1)$ state [40]. The evidence for the $(4_1^+,1)$ state is from Refs. [39, 41].

D. The cross-shell data

The cross-shell energy levels included in the least-squares fits are listed in Tables IV, V, and VI. As for the $0p$ shell, most of the entries in Tables IV and V are taken from the compilations of Ajzenberg-Selove [35] and are straightforward. Here we comment on the exceptions to this rule. The entry Δ_{sfp} in Table IV is a perturbative correction for the effects of the $0s$ and $0f1p$ shells. This correction will be described in Sec. V B. The neutron-rich nuclei listed in Table VI are also included in the fits. They are considered in Sec. VI A.

1. $1\hbar\omega$ states

^{10}B. We include all odd-parity T=0 states with $E_x(^{10}\text{B})<7$ MeV and T=1 states with $E_x(^{10}\text{Be})<9.3$ MeV. The binding energy of the ^{10}Li $(2_1^-,2)$ state (No. 9) is taken from the observed anomaly at 21.22 MeV in ^{10}Be [35].

^{11}B. All even-parity states with $E_x(^{11}\text{B})<11.2$ MeV are included.

^{12}C. All odd-parity T=0 levels below 14 MeV in ^{12}C and T=1 levels below 5.9 MeV in ^{12}B are included.

^{13}C. All even-parity states below 10.4 MeV in ^{13}C are included. The $1\hbar\omega$ $(\frac{3}{2}_1^+,\frac{3}{2})$ state of mass 13 (No. 37) is identified with the ^{13}B 3483-keV state which is experimentally assigned $J^\pi=(\frac{1}{2},\frac{3}{2},\frac{5}{2})^+$.

^{14}N. All odd-parity T=0 levels below 9.2 MeV in ^{14}N and T=1 levels below 10.0 MeV in ^{14}C are included as well as the $(4_1^-,1)$ and $(5_1^-,1)$ states (Nos. 50–51) identified in the (p,π^+) reaction [42]. The $(2_1^-,2)$ state (No. 52) is taken to lie at 22.1 MeV in ^{14}C. The other T=2 states (Nos. 53–56) are assumed to have the spin-parity

values listed as most probable by Ajzenberg-Selove.

^{15}N. The $1\hbar\omega$ states of ^{15}N were examined in detail by Alburger and Millener [43] and earlier by Lie, Engeland, and Dahll [19]. The cutoff of $E_x(^{15}\text{N})$=8.4 MeV for the $T = \frac{1}{2}$ states follows the consensus that states above this energy are likely to have large $3\hbar\omega$ components.

^{16}O. It is expected that the E_x of the T=0 $0_1^- - 3_1^-$ quartet are rather strongly affected by interaction with $\geq 3\hbar\omega$ states. Nevertheless these states are included in the fits because of their relatively simple $1\hbar\omega$ structure.

TABLE IV. The 146 $1\hbar\omega$ states used in the cross-shell fits. The factor Δ_{sfd} corrects for neglect of the $0s$ and $0f1p$ shells. It is discussed in Sec. IV B. The last two columns are the results of the PSDT interaction. The last column is experiment (Expt.) − theory for E_x.

No.	Nucleus	$2J^\pi$	$2T$	k	E_x (MeV) Δ_{sfp}	Expt.	Theory	Δ	No.	Nucleus	$2J^\pi$	$2T$	k	E_x (MeV) Δ_{sfp}	Expt.	Theory	Δ
1	^{10}B	4^-	0	1	0.136	5.110	5.188	−0.078	51	^{14}N	10^-	2	1	0.000	17.183	17.044	0.139
2	^{10}B	6^-	0	1	0.075	6.127	6.312	−0.185	52	^{14}N	4^-	4	1	0.000	24.413	24.425	−0.012
3	^{10}B	8^-	0	1	0.026	6.560	6.587	−0.027	53	^{14}N	2^-	4	1	0.000	25.153	25.617	−0.464
4	^{10}B	2^-	0	1	0.356	6.873	6.835	0.038	54	^{14}N	6^-	4	1	0.000	25.793	25.902	−0.109
5	^{10}B	2^-	2	1	0.417	7.700	7.559	0.141	55	^{14}N	4^-	4	2	0.000	26.273	26.480	−0.207
6	^{10}B	4^-	2	1	0.179	8.003	8.296	−0.293	56	^{14}N	8^-	4	1	0.000	26.493	26.171	0.322
7	^{10}B	6^-	2	1	0.018	9.111	9.147	−0.036	57	^{15}N	5^+	1	1	0.000	5.270	5.132	0.138
8	^{10}B	8^-	2	1	0.023	11.010	11.168	−0.158	58	^{15}N	1^+	1	1	0.239	5.299	5.380	−0.081
9	^{10}B	4^-	4	1	0.268	22.960	23.016	−0.056	59	^{15}N	5^+	1	2	0.000	7.155	7.545	−0.390
10	^{11}B	1^+	1	1	0.395	6.792	6.892	−0.100	60	^{15}N	3^+	1	1	0.000	7.301	7.035	0.266
11	^{11}B	5^+	1	1	0.019	7.286	6.954	0.332	61	^{15}N	7^+	1	1	0.000	7.567	7.565	0.002
12	^{11}B	3^+	1	1	0.021	7.978	8.412	−0.434	62	^{15}N	1^+	1	2	0.018	8.313	8.668	−0.355
13	^{11}B	7^+	1	1	0.033	9.185	8.793	0.392	63	^{15}N	1^+	3	1	0.000	11.615	11.889	−0.274
14	^{11}B	5^+	1	2	0.608	9.274	8.783	0.491	64	^{15}N	5^+	3	1	0.000	12.355	12.551	−0.196
15	^{11}B	3^+	1	2	0.213	9.876	9.812	0.064	65	^{16}O	6^-	0	1	0.000	6.130	6.621	−0.491
16	^{11}B	7^+	1	2	0.022	10.597	10.191	0.406	66	^{16}O	2^-	0	1	0.000	7.117	7.750	−0.633
17	^{11}B	1^+	3	1	0.296	12.534	13.094	−0.560	67	^{16}O	4^-	0	1	0.000	8.872	8.932	−0.060
18	^{11}B	5^+	3	1	0.031	14.312	14.526	−0.214	68	^{16}O	0^-	0	1	0.000	10.957	10.820	0.137
19	^{12}C	6^-	0	1	0.000	9.641	10.022	−0.381	69	^{16}O	4^-	2	1	0.000	12.896	13.129	−0.233
20	^{12}C	2^-	0	1	0.192	10.844	10.922	−0.078	70	^{16}O	0^-	2	1	0.000	13.016	13.080	−0.064
21	^{12}C	4^-	0	1	0.028	11.828	12.305	−0.477	71	^{16}O	6^-	2	1	0.000	13.194	13.621	−0.427
22	^{12}C	8^-	0	1	0.000	13.352	13.692	−0.340	72	^{16}O	2^-	2	1	0.000	13.293	13.486	−0.193
23	^{12}C	4^-	2	1	0.083	16.784	16.899	−0.115	73	^{16}O	8^-	0	1	0.000	17.775	17.885	−0.110
24	^{12}C	2^-	2	1	0.418	17.731	17.600	0.131	74	^{16}O	8^-	2	1	0.000	19.067	19.388	−0.321
25	^{12}C	6^-	2	1	0.004	18.498	18.564	−0.066	75	^{17}O	9^-	1	1	0.000	5.218	5.450	−0.232
26	^{12}C	2^-	2	2	0.449	19.411	18.951	0.460	76	^{17}O	11^-	1	1	0.000	7.757	7.782	−0.025
27	^{12}C	4^-	2	2	0.120	19.570	18.604	0.966	77	^{17}O	9^-	1	2	0.000	8.885	8.537	0.348
28	^{12}C	8^-	2	1	0.000	19.628	18.950	0.678	78	^{17}O	13^-	1	1	0.000	15.780	15.558	0.222
29	^{12}C	6^-	2	2	0.020	20.836	20.331	0.505	79	^{17}O	1^-	3	1	0.000	11.079	10.365	0.714
30	^{13}C	1^+	1	1	0.264	3.089	2.671	0.418	80	^{17}O	3^-	3	1	0.000	12.453	12.306	0.147
31	^{13}C	5^+	1	1	0.000	3.854	3.662	0.192	81	^{17}O	5^-	3	1	0.000	12.986	12.692	0.294
32	^{13}C	5^+	1	2	0.082	6.864	7.044	−0.180	82	^{17}O	7^-	3	1	0.000	14.202	14.213	−0.011
33	^{13}C	7^+	1	1	0.000	7.492	7.707	−0.215	83	^{17}O	3^-	3	2	0.000	14.283	14.461	−0.178
34	^{13}C	3^+	1	1	0.008	7.686	7.556	0.130	84	^{17}O	1^-	3	2	0.000	14.742	13.924	0.818
35	^{13}C	3^+	1	2	0.318	8.200	7.901	0.299	85	^{17}O	5^-	3	2	0.000	14.985	15.077	−0.092
36	^{13}C	9^+	1	1	0.000	9.500	9.703	−0.203	86	^{17}O	5^-	3	3	0.000	15.494	15.567	−0.073
37	^{13}C	3^+	3	1	0.030	18.591	18.680	−0.089	87	^{18}F	0^-	0	1	0.187	1.081	1.293	−0.212
38	^{13}C	1^+	5	1	0.000	34.502	34.080	0.422	88	^{18}F	4^-	0	1	0.152	2.101	1.975	0.126
39	^{14}N	0^-	0	1	0.146	4.915	4.522	0.393	89	^{18}F	2^-	0	1	0.182	3.134	3.319	−0.185
40	^{14}N	4^-	0	1	0.000	5.106	4.510	0.596	90	^{18}F	6^-	0	1	0.217	3.791	3.489	0.302
41	^{14}N	2^-	0	1	0.320	5.691	5.086	0.605	91	^{18}F	4^-	0	2	0.165	4.226	4.575	−0.349
42	^{14}N	6^-	0	1	0.000	5.834	5.930	−0.096	92	^{18}F	8^-	0	1	0.219	4.398	4.693	−0.295
43	^{14}N	4^-	0	2	0.000	7.967	8.169	−0.202	93	^{18}F	10^-	0	1	0.408	4.848	5.179	−0.331
44	^{14}N	2^-	2	1	0.069	8.407	7.839	0.568	94	^{18}F	2^-	0	2	0.086	4.860	5.461	−0.601
45	^{14}N	8^-	0	1	0.000	8.490	8.911	−0.421	95	^{18}F	6^-	0	2	0.224	5.502	5.609	−0.107
46	^{14}N	6^-	2	1	0.116	9.041	8.588	0.453	96	^{18}F	14^-	0	1	0.003	7.240	7.094	0.146
47	^{14}N	0^-	2	1	0.083	9.216	9.337	−0.121	97	^{18}F	2^-	2	1	0.191	5.498	5.608	−0.110
48	^{14}N	4^-	2	1	0.000	9.654	9.078	0.576	98	^{18}F	6^-	2	1	0.285	6.140	6.154	−0.014
49	^{14}N	6^-	2	2	0.000	12.114	12.229	−0.115	99	^{18}F	4^-	2	1	0.086	6.572	6.287	0.285
50	^{14}N	8^-	2	1	0.000	13.979	14.019	−0.040	100	^{18}F	2^-	2	2	0.424	7.240	8.237	−0.997

TABLE IV. (*Continued*).

No.	Nucleus	$2J^\pi$	$2T$	k	Δ_{sfp}	E_x (MeV) Expt.	Theory	Δ	No.	Nucleus	$2J^\pi$	$2T$	k	Δ_{sfp}	E_x (MeV) Expt.	Theory	Δ
101	^{18}F	4^-	2	2	0.263	7.393	7.394	−0.001	124	^{19}F	5^-	1	2	0.192	4.683	4.360	0.323
102	^{18}F	6^-	2	2	0.086	7.446	7.336	0.110	125	^{19}F	7^-	1	2	0.224	5.418	5.064	0.354
103	^{18}F	0^-	2	1	0.031	7.922	7.893	0.029	126	^{19}F	5^-	1	3	0.243	5.621	5.645	−0.024
104	^{18}F	2^-	2	3	0.389	8.661	8.483	0.178	127	^{19}F	3^-	1	3	0.248	6.088	5.774	0.314
105	^{18}F	4^-	2	3	0.141	8.813	8.606	0.207	128	^{19}F	9^-	1	2	0.010	6.100	5.570	0.530
106	^{18}F	10^-	2	1	0.184	8.906	9.035	−0.129	129	^{19}F	7^-	1	3	0.429	6.161	5.975	0.186
107	^{18}F	8^-	2	1	0.182	9.019	9.095	−0.076	130	^{19}F	1^-	1	2	0.180	6.429	6.579	−0.150
108	^{18}F	2^-	2	4	0.385	9.081	8.796	0.285	131	^{19}F	11^-	1	1	0.126	7.166	6.841	0.325
109	^{18}F	10^-	2	2	0.365	9.167	9.406	−0.239	132	^{19}F	13^-	1	1	0.147	8.288	8.207	0.081
110	^{18}F	6^-	2	3	0.701	9.324	9.503	−0.179	133	^{19}F	11^-	1	2	0.434	8.953	8.600	0.353
111	^{18}F	8^-	2	2	0.100	9.452	9.746	−0.294	134	^{19}F	1^-	5	1	0.000	22.323	22.015	0.308
112	^{18}F	14^-	2	1	0.000	12.172	12.169	0.003	135	^{20}Ne	4^-	0	1	0.215	4.967	5.195	−0.228
113	^{18}F	2^-	4	1	0.000	17.326	17.703	−0.377	136	^{20}Ne	6^-	0	1	0.207	5.621	5.622	−0.001
114	^{18}F	4^-	4	1	0.000	17.441	17.361	0.080	137	^{20}Ne	8^-	0	1	0.172	7.004	7.139	−0.135
115	^{18}F	4^-	4	2	0.000	17.913	18.006	−0.093	138	^{20}Ne	10^-	0	1	0.177	8.453	8.398	0.055
116	^{18}F	6^-	4	1	0.000	18.073	18.016	0.057	139	^{20}Ne	12^-	0	1	0.146	10.609	10.224	0.385
117	^{18}F	8^-	4	1	0.000	19.742	19.791	−0.049	140	^{20}Ne	14^-	0	1	0.132	13.338	12.621	0.717
118	^{19}F	1^-	1	1	0.133	0.110	0.223	−0.113	141	^{20}Ne	16^-	0	1	0.280	15.700	15.028	0.672
119	^{19}F	5^-	1	1	0.213	1.346	1.754	−0.408	142	^{20}Ne	6^-	4	1	0.323	22.407	22.325	0.082
120	^{19}F	3^-	1	1	0.159	1.459	1.926	−0.467	143	^{20}Ne	10^-	4	1	0.287	24.045	24.442	−0.397
121	^{19}F	7^-	1	1	0.185	3.999	4.453	−0.454	144	^{20}Ne	4^-	6	1	0.000	36.887	36.830	0.057
122	^{19}F	9^-	1	1	0.171	4.033	4.203	−0.170	145	^{21}Ne	1^-	7	1	0.000	38.906	38.753	0.153
123	^{19}F	3^-	1	2	0.274	4.556	4.736	−0.180	146	^{22}Na	0^-	8	1	0.000	48.637	48.332	0.305

TABLE V. Nine $2\hbar\omega$ levels used in the cross-shell fits. The last two columns give the results of the MI-LC least-squares fit to the 216 A=10–22 states resulting in the cross-shell interaction PSDT. The index k orders the states of given (J^π, T) in energy. Δ is experiment (Expt.) − theory for E_x.

No.	Nucleus	$2J^\pi$	$2T$	k	E_x (MeV) Expt.	Theory	Δ
1	^{15}N	15^-	1	1	21.500	21.190	0.310
2	^{16}O	12^+	0	1	14.815	15.083	−0.268
3	^{16}O	14^+	2	1	26.996	27.314	−0.318
4	^{16}O	0^+	4	1	22.721	22.115	0.606
5	^{16}O	4^+	4	1	24.487	24.485	0.002
6	^{16}O	0^+	4	2	25.748	25.527	0.221
7	^{16}O	4^+	4	2	26.883	27.049	−0.166
8	^{16}O	6^+	4	1	26.809	27.806	−0.997
9	^{16}O	8^+	4	1	27.039	27.151	−0.112

TABLE VI. T_z=0 or $+\frac{1}{2}$ analogues of $T = T_z$ exotic neutron-rich nuclei used in the cross-shell fits. The index k orders the states of given (J^π, T) in energy. Δ is experiment (Expt.) − theory for E_x. The extraction of E_x from the $E_{B_{\rm exp}}$ of the $T = T_z$ nuclei is described in Sec. VI A. The limits for Nos. 4 and 10 correspond to $S(2n)$=0 (see Sec. VI A).

No.	Nucleus	$2J^\pi$	$2T$	k	E_x (MeV) Expt.	Theory	Δ
1	^{14}N	0^+	6	1	41.524	41.670	−0.146
2	^{15}N	3^-	5	1	32.219	31.955	0.264
3	^{17}O	3^-	7	1	50.055	49.665	0.390
4	^{19}F	3^-	9	1	≤69.206	69.696	−0.490
5	^{17}O	3^+	5	1	26.094	26.147	−0.053
6	^{18}F	0^+	6	1	30.914	30.443	0.471
7	^{18}F	4^+	6	1	32.534	32.606	−0.072
8	^{19}F	1^+	7	1	41.088	41.675	−0.587
9	^{20}Ne	0^+	8	1	54.334	54.247	0.087
10	^{22}Na	0^+	10	1	≤72.114	72.247	−0.133

We include all T=0,1 yrast states with $J \leq 4$. The $(4_1^-, 0)$ state is identified in the (e, e') reaction [44]. E_x for the analogue of the ^{16}N ground state (No. 69) was taken from the difference in the centroid energies of the E_x for the low-lying T=1 quartet in ^{16}N and ^{16}O. The ^{16}O $(4_1^-, 1)$ state (No. 74) is discussed by Hyde-Wright *et al.* [44] and Saha *et al.* [45].

^{17}O. The mixing of the $T = \frac{1}{2}$ $1\hbar\omega$ and $3\hbar\omega$ states in ^{17}O is unusually large and complex and, at the present time, is not well understood [17, 46, 47]. The influence of the $0f1p$ shell is also not well understood [46]. For these reasons we choose to include only the $T = \frac{1}{2}$, $\frac{9}{2}^-$, $\frac{11}{2}^-$, and $\frac{13}{2}^-$ states listed in Table IV. The last of these is from the (p, π^+) study of Ref. [48]. The $T = \frac{3}{2}$ $1\hbar\omega$ states — the ground-state configuration for ^{17}N — are better in hand. The $3\hbar\omega$ states are estimated to commence at ~6.4 MeV excitation in ^{17}N [49]. Our identification of the ^{17}N $1\hbar\omega$ states follows that shown in Fig. 2 of Ref. [49] and we include in the fit all nine experimental levels below $E_x(^{17}\text{N})$=5.0 MeV shown in that figure.

^{18}F. The $3\hbar\omega$ states are estimated to commence at ~6.4 and ~9.5 MeV for T=0 and 1, respectively [50]. The nine odd-parity T=0 states with $E_x \leq 5502$ keV listed by Ajzenberg-Selove were included in the fit. Likewise, all fourteen odd-parity states with $E_x(^{18}\text{O})$<8.4 MeV were included [the 7977-keV level of ^{18}O was taken to be the $(4_1^-, 1)$ state]. In addition, the $(7_1^-, 0)$ and $(7_1^-, 1)$ states at 7240 keV in ^{18}F [51] and 11130 keV in ^{18}O [50] and the $(4_2^-, 1)$ state were included. The latter — located at 8410 keV in ^{18}O [52, 53] — was considered important because it and the $(5_1^-, 2)$ state comprise $[p_{1/2}^{-1} \otimes (sd)^3_{9/2,T_{sd}}]_{4^-,5^-}$ doublets with the yrast 4^- and 5^- states — the yrast states being mainly $T_{sd} = \frac{1}{2}$, and the yrare states $T_{sd} = \frac{3}{2}$.

As can be seen from Table IV, all these states have small and relatively similar Δ_{sfp} correction factors. The T=2 states are discussed by Millener [54].

^{19}F. The estimated onset of $3\hbar\omega$ states is ~9.2 MeV [17]. All odd-parity states with $E_x \leq 7.5$ MeV are included in the table along with the $(\frac{13}{2}^-_1, \frac{1}{2})$ and $(\frac{11}{2}^-_2, \frac{1}{2})$ states.

^{20}Ne. Of all states considered, the $1\hbar\omega$ states of A=20 represent the severest test of the computer resources. Some T=0 levels were included in the fit. The dimensions of the T=1 levels are larger and these were not included. The J^π=2^- – 7^- states listed in Table III belong to the K^π=2^- band [35]. They have uniform and small values of Δ_{spf}. Odd-parity states at 5788 and 7156 keV are assigned to the K^π=0^- band. Since this band has a large $0f1p$ component [53], these states were not included in the fit.

2. $2\hbar\omega$ states

In Table V, the ^{15}N $\frac{15}{2}^-$ and ^{16}N $(7_1^+,1)$ states (Nos. 1 and 3) are from the (p, π^+) work of Aziz [48]. The analogue of the ^{16}C ground state (No. 4) is known to lie at 22.721 MeV in ^{16}O. The excitation energies of the five other T=2 states in ^{16}O (Nos. 5–9) are taken from the ^{16}C spectrum. We assume 2_2^+ and 3_1^+ for the ^{16}C states at 3986 keV (No. 7) and 4088 keV (No. 8). (Note that with our final interaction the odd-parity $3\hbar\omega$ spectrum of ^{16}C commences at 5.1 MeV).

IV. PRELIMINARIES AND PROCEDURES

A. The scope of the fits

The final fits include levels in the A=10–22 region. The region A=5–9 was avoided because it has been long known [55] that there is considerable cluster structure in this mass region and we wished to avoid the prejudicing of the interaction by this structure. Also the influence of the $0s$ shell will be more strongly felt in the lightest of these nuclei. The upper limit was chosen because as A increases much above A=20 we expect the influence of the $0f1p$ shell on the (1–2)$\hbar\omega$ states to become rapidly stronger so that a proper treatment of most $A > 20$ states — and some states in $A \leq 20$ nuclei as well — involves the $0f1p$ shell. Also, the dimensions to be diagonalized and otherwise treated are becoming uncomfortably large above A=19. Given the restriction to A=10–22 nuclei, there is still some influence on the $1\hbar\omega$ states from the $0s$ and $0f1p$ shells. As will be described, we handle this influence perturbatively. Like the Millener-Kurath interaction, our interaction contains three separable parts: (1) a $0p$-shell interaction, (2) a cross-shell $0p1s0d$-interaction, and (3) a $1s0d$ interaction. In a weak-coupling spirit, we take the TBME and SPE of (3) from the W interaction and describe the TBME of the $0p$-shell and cross-shell interactions by two completely separate interactions. The parameters to be varied are the TBME or potentials describing (1) and (2) plus the SPE parameters of the $0p$ shell. Note that unlike the $1s0d$-shell interaction, the $0p$-shell interaction is not taken as fixed. This is done for two reasons: first, it is hoped that the additional data from $>0\hbar\omega$ states will help to determine the $0p$-shell interaction, and second, it was expected that there would be some departure from strict weak coupling, i.e., the optimum $0p$-shell interaction for an overall fit to $0p + 0p1s0d$ states is expected to be somewhat different than the optimum interaction for the $0p$ shell alone. We include some $2\hbar\omega$ states in the fit but assume no mixing between $0\hbar\omega$ and $2\hbar\omega$ states. This is in the same spirit as the customary neglect of $>0\hbar\omega$ admixtures in the fits to $0\hbar\omega$ states within a major shell. (0+2)$\hbar\omega$ mixing is not included because of the difficulty of dealing with the well-known "$n\hbar\omega$ truncation catastrophe" which occurs when such mixing is attempted [56, 57]. In general, $2\hbar\omega$ excitations include 1p-1h (1 particle–1 hole) excitations through two major shells as well as 2p-2h excitations through one major shell. [With $\mathcal{N}$ the principal quantum number ($\mathcal{N}$=0,1,2,...) Q=$2\mathcal{N} + l$ is the number of quanta in a major shell. Then a $n\hbar\omega$ excitation has $\Delta Q \leq n$ contributions.] A difficult problem in the treatment of the $2\hbar\omega$ excitations when both 2p-2h and 1p-1h excitations are allowed is the elimination of spuriosity and the maintenance of a proper balance between the potential and kinetic energy contributions so

that the Hartree-Fock condition is adequately satisfied and the centroid of the monopole strength is placed at a reasonable position (~20–30 MeV) [57]. We avoid this problem by only including $2\hbar\omega$ states which — by virtue of high spin or isospin — can have no contributions from 1p-1h excitations.

B. The potential representation

In its general form the potential we use to represent the residual interaction consists of the standard one-boson-exchange potential (OBEP) of Hosaka, Kubo, and Toki (HKT) [33] described in Sec. III E of BRJW plus the multipole interaction described in Sec. III F of BRJW. Exhaustive tests of the sensitivity of the results to the various possible parameters were made for both the $0p$ shell and the cross shell. The form of the interaction used in the final fits was arrived at on the basis of these studies and those reported by BRJW. In the sections to come, we will distinguish the potential fits by the number of potential parameters, n_p, the number of SPE parameters, $n_{\rm spe}$, and the assumed mass dependence of the interaction:

$$\langle V(A)\rangle = \langle V(16)\rangle\left(\frac{A}{16}\right)^{-p_A}. \tag{2}$$

The standard $0p$-shell potential, POT($n_p, n_{\rm spe}, p_A$), has either $n_{\rm spe} = 2$ (no mass dependence) or $n_{\rm spe} = 4$ (linear mass dependence) with the SPE given in either case by

$$\epsilon_j(A) = \epsilon_j(5) + \frac{A-5}{10}\Delta\epsilon_j, \tag{3}$$

with the $\Delta\epsilon_j$ ($j = \frac{1}{2}, \frac{3}{2}$) held fixed at 0 for $n_{\rm spe}$=2. We note that other forms of the mass dependence were explored but none were found that gave significantly better fits to the $0p$-shell or cross-shell data.

The POT($n_p, n_{\rm spe}, p_A$) for both the $0p$-shell and cross-shell interactions has the following general properties:

(1) Following BRJW, the four [(ST)=(00), (10), (01), (11)] central long-range (1.414 fm) standard one-pion exchange potential (OPEP) terms were held fixed at their HKT values as was the (ST)=(11) tensor OPEP term.

(2) The remaining central contribution in each of the four (ST) channels was taken as (see Sec. III E of BRJW)

$$d_c(r_{12}, S, T) = A_c(ST)\sum_i \alpha_{\rm HKT}(S, T, i)\exp(-x_i)/x_i, \tag{4}$$

where the x_i are r_{12} divided by the interaction range μ_i which takes on the values 0.2, 0.33, and 0.5 fm in Eq. (4). Thus we assume the relative contributions, $\alpha_{\rm HKT}(S, T, i)$, determined by HKT for the three ranges and treat their overall strength, $A_c(ST)$, as a variable. The two μ_i terms (=0.25 and 0.40 fm) in the spin-orbit contribution were treated in a similar fashion. The HKT tensor contribution has only one range component other than the long-range one.

(3) A variable monopole term was added in each of the four central channels. No improvement was found in the fits with both a central and monopole term in the (ST)=(00) and (11) channels. Thus the (00) and (11) central terms were fixed at the HKT values, i.e., $A_c(00) = A_c(11) = 1.0$.

(4) Attempts to improve the fits by adding higher multipoles to the four central channels were made for both the $0p$-shell (quadrupole only) and cross-shell (dipole, quadrupole, and octupole) interactions. No improvement was found for the $0p$ shell. The HKT potential can be decomposed into multipole components and so from a mathematical point of view the multipole interaction introduced by BRJW does not contribute any new terms, rather it provides a mechanism for changing the relative weighing of the various allowed multipoles. Thus it is as expected that the quality of the $0p$-shell fit is not improved with the addition of "monopole + quadrupole" terms in the four central channels beyond that already achieved with monopole terms. For the cross-shell interaction, various combinations of all allowed multipoles — monopole, dipole, quadrupole, and octupole — were included in the fit. The addition of "monopole + quadrupole" in the (ST)=(10) central channel improved the fit slightly over that for monopole alone, and "monopole + octupole" in all four central channels gave a marginally improved fit. Neither improvement was enough to warrant the extra complexity (and thus loss of interpretability) and the results we present have — as multipole variables — monopole terms only in each of the four (ST) central channels. No multipole terms were included in the tensor or LS components because their addition brought about no significant improvement in the fits.

(5) The influence of the density dependence of Eq. (26) of BRJW (with $A_d = -1$, $B_d = 1$) was studied for the central terms of Eq. (4). Introducing this density dependence caused a slight improvement in the fits to the cross-shell data. However we have adopted the density-independent form because the greater interpretability of the results outweighs the slight loss of accuracy. Note that since only $0p$ orbits are involved, the density dependence has no effect on the $0p$-shell results.

(6) With the above assumptions, there are a total of eighteen contributions to the potential with seven held fixed. The spin-orbit (10) term was found to be very poorly determined in both the $0p$- and cross-shell fits. Thus, in the final fits it too was held fixed resulting in a 10-variable potential. However some of the preliminary results we shall present were obtained with an 11-variable potential.

C. First-principle-interactions

There exist considerable theoretical guidance of a relatively fundamental nature for the $0p$-shell interaction. Here we consider three interactions based on nucleon-nucleon scattering data. These are the G-matrix interactions of Kuo [58] and Bertsch *et al.* [59] as well as the HKT interaction already discussed. We shall designate these as the KUO, M3Y, and HKT bare G-matrix interactions [60, 61]. In addition Kuo [58] has recently recalculated the core-polarization corrections as well as

the G-matrix interaction starting from the Paris nucleon-nucleon potential [62] so that he provides a complete first-principles interaction. The two-body matrix elements of these interactions are listed in Table VII. Table VII is given to illustrate two points: (1) although the three bare G-matrix interactions have obvious similarities, there are also noticeable differences, and (2) the core-polarization contribution is appreciable. Further information can be obtained from a spin-isospin decomposition of these interactions.

In the $0p$ shell, a complete LS spin-isospin decomposition of the jj-coupled TBME can be made in terms of the eleven potential parameters described in the last subsection together with four antisymmetric spin-orbit (ALS) terms (see Sec. II D of BRJW). The bare G-matrix interactions contain no ALS terms and so the potential representation described in the last subsection provides a complete LS set for their description. The results of these spin-isospin decompositions are given in Table VIII where the results are expressed in terms of the strengths of the eleven possible terms relative to those of the standard HKT plus monopole potential. This table defines the eleven parameters used in the potential fits and illustrates the range of values which can be expected for the potential variables. It can be seen that the variation of the potential parameters between the four interactions is considerably larger than the variation between the TBME listed in Table VII. This illustrates an important point: namely, it is the combined contribution for a given channel that is important in determining the TBME, and the combined contribution to, say, the (10) tensor channel is a complex function of the two individual contributions. For this reason it is difficult to compare potential parameters arrived at from different fits.

In applying the MI-LC least-squares method a "background" interaction is used to evaluate those linear combinations which are not well determined. We thus have need for a "first-principles" interaction with its strength and SPE tuned to the $0p$ shell. Such an interaction is constructed by a least-squares fit of the KUO interaction to the 51 A=10–16 or 86 A=5–16 binding energies described in Sec. III C. The variables are the two SPE and the overall strengths of the bare G-matrix A_G and core polarization A_{cp} contributions. For no mass dependence of the interaction, the A=5–16 fit yields A_G=1.00±0.02, A_{cp}=1.04±0.05, $\epsilon_{3/2}$=1.200 MeV, and $\epsilon_{1/2}$=3.902 MeV. The fit has $E^{(p)}_{\rm rms}$=1.176 MeV where we use the following standard definition as a measure of the goodness of fit,

$$[E^{(\alpha)}_{\rm rms}]^2 = \sum_i^{N_d} [E_i(\text{exp}) - E_i(\text{th})]^2/N_d, \tag{5}$$

with E(exp) and E(th) being the experimental and fitted theoretical binding energies and N_d the number of datum. The index α specifies the model space. It is seen that the strength of the Kuo interaction is well tuned to the $0p$ shell. We are interested in a mass-independent interaction for use with a A=10–16 MI-LC fit. A fit to this region with A_G and A_{cp} held fixed at unity yields $\epsilon_{3/2}$=1.128 MeV, $\epsilon_{1/2}$=4.449 MeV, and $E^{(p)}_{\rm rms}$=1.312 MeV. The Kuo "bare + core-polarization" interaction PKUO with these SPE provides the "background" interaction for the MI-LC least-squares fit to the A=10–16 p-shell energies.

D. Tests of the fitting procedure

We first ask whether our $0p$-shell data sets are adequate to determine the interaction. To address this question the set of 51 A=10–16 level binding energies was generated with the Kuo interaction, PKUO, and this was taken as

TABLE VII. Three bare G-matrix p-shell interactions. The last column is Kuo's core-polarization contribution.

$2j_1$	$2j_2$	$2j_3$	$2j_4$	J	T	Two-body matrix elements (MeV)			
						HKT	M3Y	KUO	
								Bare	Core pol.
1	1	1	1	1	0	−2.7890	−2.8730	−2.8210	0.2886
1	1	1	1	0	1	−0.5227	−0.3197	−0.0070	−0.0653
1	1	3	1	1	0	1.6724	1.8127	2.2030	0.1112
1	1	3	3	1	0	2.2648	2.0737	2.7560	−1.0033
1	1	3	3	0	1	−3.6213	−3.7905	−4.4760	0.5163
3	1	3	1	1	0	−6.7864	−6.9056	−7.0510	−0.1945
3	1	3	1	2	0	−6.4982	−6.5611	−8.0080	1.4963
3	1	3	1	1	1	−0.5955	−0.2560	−0.8130	1.4557
3	1	3	1	2	1	−2.4815	−2.3923	−3.2880	2.2112
3	1	3	3	1	0	4.7930	4.6241	5.4320	−0.3701
3	1	3	3	2	1	−1.6009	−1.7321	−1.9580	0.0713
3	3	3	3	1	0	−1.9994	−2.0176	−1.4380	−0.9684
3	3	3	3	3	0	−5.2569	−5.5921	−6.2060	0.5197
3	3	3	3	0	1	−3.0833	−3.0000	−3.1720	−0.2161
3	3	3	3	2	1	−1.3495	−1.1675	−1.9030	1.0738

TABLE VIII. The 4th through 6th columns give potential parameters (in MeV) resulting from a spin-isospin decomposition of the three bare G-marix interactions discussed in the text. The 7th column is the result of a POT(11,2,0.0) fit to the "bare + core-polarization" interaction PKUO. This fit gave $E_{\rm rms}^{(p)}$=291 keV (121 keV with mass-dependent SPE) for 51 A=10–16 levels. Results are given relative to the strengths of the HKT potential parameters. Parameters held fixed are indicated by "1" and are not given a variable number. The eighteen parameters are those discussed in Sec. III B. The entry under "Form" is from Table VI of BRJW.

Component	ST	Form[a]	HKT	M3Y	KUO	PKUO	Variable
Central	00	DI–HSM3	1	1	1	1	
		DI–FOPEP	1	1	1	1	
		monopole	0.000	−0.246	1.276	−2.411	1
	01	DI–HSM3	1.000	1.025	0.718	2.013	2
		DI–FOPEP	1	1	1	1	
		monopole	0.000	0.059	−1.763	3.508	3
	10	DI–HSM3	1.000	0.881	0.826	1.092	4
		DI–FOPEP	1	1	1	1	
		monopole	0.000	−0.732	0.302	0.350	5
	11	DI–HSM3	1	1	1	1	
		DI–FOPEP	1	1	1	1	
		monopole	0.000	−1.818	−0.115	1.097	6
Tensor	10	DI–S2	1.000	0.469	2.122	−0.863	7
		DI–OPEP	1.000	0.889	1.536	0.825	8
	11	DI–S2	1.000	1.044	−0.169	1.701	9
		DI–FOPEP	1	1	1	1	
Spin-orbit	11	DI–HSM3	1.000	1.086	1.916	0.855	10
	10	DI–HSM3	1.000	−3.309	−0.650	−8.484	11

[a] DI=density independent; DI=density dependent; FOPEP means the standard long-range pion exchange component was held fixed. The other terms are easily recognized from the discussion of Sec. III B.

the "experimental" data set in fits to (a) the "15 TBME + 2 SPE" parameter set and (b) the POT(11,4,0.2) potential. The starting interaction for the fits was a surface delta interaction (SDI) with the experimental SPE of ^{5}He. For (a), the iterative procedure of steps (1) through (4) of Sec. III A of BRJW converged to an accuracy of <1 keV error in all 17 parameters after 7 iterations. For (b), the iterative procedure converged to $E_{\rm rms}^{(p)}$=121 keV in 5 iterations. If now we mix (a) and (b) by 3 iterative steps with (b) before fitting with (a), we achieved the <1 keV error in 5 iterations rather than the 7 it took with (a) alone. The difference in the $E_{\rm rms}^{(p)}$ between fits (a) and (b) reflects the fact that (a) provides a complete representation of the input data while (b) does not.

A more realistic test is to add a different random error to each "experimental datum" before the fit. We used $300x_r$ keV for this error where x_r is a random number between −1 and +1. The iterative process did not find the correct minimum when using the TBME search [method (a)]; it stuck at $E_{\rm rms}^{(p)} \approx 500$ keV. However, if POT(11,4,0.2) fits were iteratively made until the solution stabilized and then method (a) was undertaken, the solution was close to that expected for $E_{\rm rms}^{(p)}$, e.g., 127 keV. Convergence took, in total, eight iterations in this case. The above tests illustrate that there is no guarantee that the iterative procedure used here and in previous studies will find the lowest minimum in what is, in general, a complicated multidimensional chi-squared surface. Our aim is to maximize the chances for convergence into the lowest minimum. The tests we have described here for the $0p$ shell suggest that the chances of finding the lowest minimum in a TBME search are greater if one starts with a potential search. Some other ways of constraining the number of variables in the initial steps would probably work as well or better.

One can imagine interactions with symmetries such that data sets which omit most of the high-lying levels will not be adequate to determine the generating interaction in such a test. However, it would be strange indeed if real nuclei had this property and the present test gives us assurance that the true minimum can be found when dealing with real nuclei.

V. RESULTS OF THE LEAST-SQUARES FITS

A. The $0p$-shell

A useful orientation is obtained by considering fits to the $0p$ shell alone before considering the total $0p1s0d$ fit. Also, we are interested in determining the "best" $0p$-shell interaction to use for the A=10–16 $0\hbar\omega$ states. The benchmark for the $0p$-shell interaction is the classic "15 TBME + 2 SPE" fit such as that of Cohen and Kurath [1]. First consider fits to the 86 A=5–16 datum for discrete values of the exponent p_A parameterizing the

mass dependence of the TBME in Eq. (2). The lowest value of $E^{(p)}_{\rm rms}$ was 576 keV for p_A=0.20. The minimum in $E^{(p)}_{\rm rms}$ versus p_A is shallow and this present result is in satisfactory agreement with the recent result of $E^{(p)}_{\rm rms}$=550 keV with the minimum at p_A=0.17 found for 77 0p-shell binding energies in A=5–16 nuclei [7]. The error matrix was examined and all linear combinations were found to be determined with satisfactory accuracy. Thus the LC method was not used. The interaction resulting from this fit is labeled P(5–16)T.

Now consider fits to the 51 A=10–16 binding energies of Table III. A "15 TBME + 2 SPE" fit with p_A=0.0 gave $E^{(p)}_{\rm rms}$=289 keV. Note the considerable improvement over the A=5–16 fit. The minimum in $E^{(p)}_{\rm rms}$ versus p_A was even more shallow than for the A=5–16 fit and $E^{(p)}_{\rm rms}$ was only marginally lower at the best value of p_A which was 0.10. It turns out that the cross-shell fit is also insensitive to p_A and so, for convenience, we choose to adopt a mass-independent A=10–16 0p-shell interaction, i.e., p_A=0.0. In the fit just described it was judged that the three (of 17) least well determined linear combinations of the MI-LC method had only marginally acceptable uncertainties. Thus the MI-LC method was used with the PKUO interaction as background. The fit stabilized after six iterations giving $E^{(p)}_{\rm rms}$=330 keV and the individual deviations from experiment shown in Table III. The resulting interaction is labeled P(10–16)T. In both the A=5–16 and 10–16 fits just described the starting interaction was that resulting from a potential fit. We now describe the potential fit to the A=10–16 region.

An equivalent formulation of the interaction is in terms of the 15 LS-coupled two-body potential parameters of the 0p shell. Four of these are antisymmetric spin-orbit (ALS) which are known to be relatively unimportant [1, 7, 5]. A fit to the remainder, i.e., a POT(11,2,p_A) fit gives $E^{(p)}_{\rm rms}$ of 406 and 398 keV at p_A=0.00 and 0.11, respectively, the latter being close to the minimum. If the A-dependent form of Eq. (3) is assumed for the SPE we obtain $E^{(p)}_{\rm rms}$ values of 306 and 316 for p_A=0.00 and 0.11, respectively. However, as was the case for a "15 TBME + 4 SPE" fit, the parameters are rather unphysical for $p_A \leq 0.15$, with large monopole terms canceling large $\Delta\epsilon_j$ terms. In summary, the mass-independent potential fit is considerably worse than the equivalent TBME fit; $E^{(p)}_{\rm rms}$=406 as compared to 289 keV. However, omission of the four ALS components in the potential (which is responsible for this difference) can be largely compensated for by the adoption of a mass dependence for the SPE [Eq. (3)] so that a POT(11,4,0.0) fit has an $E^{(p)}_{\rm rms}$ value, 306 keV, not much different than the "best" "TBME + 2 SPE" value of 289 keV. Nevertheless, we adopt the "TBME + 2 SPE" p-shell interactions P(5–16)T and P(10–16)T and, as will be described, use the "TBME + 2 SPE" form for the 0p-shell in our fits to the total set of A=10–22 binding energies to determine the cross-shell interaction. This decision is made (1) because use of mass-dependent SPE obfuscates the interpretation of the final fitting parameters, (2) causes undue complexity in the matching of the three parts of the cross-shell interaction, and (3) does not provide as linearly independent a set of parameters as the "TBME + 2 SPE" set.

B. The cross shell

After many initial tests using various combinations of TBME (MI) and potential (MD) parameterizations of the 0p-shell and cross-shell interactions with and without the LC method, we settled on a penultimate fit with a "15 TBME + 2 SPE" representation of the 0p-shell interaction and a POT(10,2,0.0) representation of the cross-shell interaction. After four iterations, a fit to 216 binding energies yielded $E^{(c)}_{\rm rms}$=389 keV for 165 cross-shell levels. In this fit the 51 p-shell binding energies of Table III were given equal weight to the 165 cross-shell binding energies and for these 51 0p-shell energies the fit yielded $E^{(p)}_{\rm rms}$=378 keV. This should be compared to $E^{(p)}_{\rm rms}$=330 keV found for the P(10-16)T interaction, i.e., some sacrifice in the representation of the A=10–16 0p-shell data results from a simultaneous optimization of the 0p-shell and cross-shell fits to A=10–22 data. We designate the resulting 0p-shell part of the interaction as PWBP and the total interaction as PSDP.

The parameters of the PSDP potential are listed in Table IX in the same format as that of Table VIII. It can be seen that the individual parameters for the (01) central channel (Nos. 2–3) and the (10) tensor channel (Nos. 7–8) are quite different from those of the HKT interaction. However, the combined effect in each of these two channels is not very different as was ascertained by calculating the contributions of individual channels to the TBME. This illustrates the point made earlier when comparing Tables VII and VIII.

The final fit was made by the MI-LC method using the same data. There are 95 TBME and 2 SPE to be determined and this is too many compared to the data set, especially since many of the cross-shell TBME are quite ill determined by this set. Thus the LC method is used. The choice of how many parameters to vary is quite subjective. An examination of the error matrix and the application of various judgements (see, e.g., Ref. [3]) as to the required accuracy for those linear combinations which are varied led us to the choice of 45 variables. With this choice, the 17 0p-shell parameters are quite well determined and, roughly speaking, this means we allow $\sim 45 - 17 = 28$ of the 80 cross-shell TBME to vary. The PSDP interaction resulting from the potential fit served as the background interaction for this iterative fit. After four iterations the MI-LC stabilized at $E^{(c)}_{\rm rms}$=330 keV with $E^{(p)}_{\rm rms}$=378 keV. Comparing these $E^{(\alpha)}_{\rm rms}$ to those of the mixed "TBME (p shell) + potential (cross shell)" fit it is seen that the cross-shell fit improves but the 0p-shell part of the fit — being already optimized — does not. The interactions resulting from this fit are designated as PWBT and PSDT.

There are two aspects of these fits and the resulting interactions which we have not yet adequately described. First, how is the W interaction describing the 1s0d shell handled? For $A \geq 16$ it is exactly the W interaction: the TBME are multiplied by $(18/16)^{0.30}$, and given an A dependence with p_A=0.30 in Eq. (2). However, for

TABLE IX. Parameters (in MeV) for the potential cross-shell interaction PSDP. The adopted form for the HKT potential is also shown for convenience. Parameters held fixed are indicated by "1" and are not given a variable number. The eighteen parameters are those discussed in Sec. III B. The entry under "Form" is from Table VI of BRJW.

Component	ST	Form[a]	HKT	PSDP	Variable
Central	00	DI–HSM3	1	1	
		DI–FOPEP	1	1	
		monopole	0.000	−1.6988	1
	01	DI–HSM3	1.000	−0.0055	2
		DI–FOPEP	1	1	
		monopole	0.000	−1.7351	3
	10	DI–HSM3	1.000	0.8082	4
		DI–FOPEP	1	1	
		monopole	0.000	−0.2559	5
	11	DI–HSM3	1	1	
		DI–FOPEP	1	1	
		monopole	0.000	1.5108	6
Tensor	10	DI–S2	1.000	−3.4267	7
		DI–OPEP	1.000	−0.5959	8
	11	DI–S2	1.000	1.4734	9
		DI–FOPEP	1	1	
Spin-orbit	11	DI–HSM3	1.000	0.9602	10
	10	DI–HSM3	1	1	

[a] DI=density independent; FOPEP means the standard long-range pion exchange component was held fixed. The other terms are easily recognized from the discussion of Sec. III B.

$A < 16$ the 63 TBME are fixed at the A=16 values. This has no effect on the fits described here but was found to give a better representation of $2\hbar\omega$ states than a simple overall p_A=0.30 dependence. We wish to use the three SPE for the $1s0d$ shell which are associated with the W interaction. However, the effective SPE for these orbits is composed of these plus sums over the cross-shell TBME, and these sums are dependent on the fits. There are several ways to handle this interdependence; for instance, it could be incorporated into the iterative procedure. We solved it simply by including the model ^{17}O $d_{5/2}$, $d_{3/2}$, and $s_{1/2}$ single-particle states and the ^{16}O ground state into the fits with overwhelmingly small assigned errors.

The second point to be elaborated on is how we account for the influence of the $0s$ and $0f1p$ shells. Ideally these orbits should be included in the fits. However this would drastically increase the magnitude of the fitting procedure and, in any case, the parameters associated with these orbits would be quite poorly determined indeed. Thus, their influence on the $1\hbar\omega$ states was added perturbatively and only $2\hbar\omega$ states with no influence from these orbits were included in the fits. The procedure was to calculate all the relevant $1\hbar\omega$ spectra with a full *spsdpf* model-space interaction, first with the active nucleons confined to the *psd* shells and second with the full $1\hbar\omega$ model space. The correction for the neglect of the $0s$ and $0f1p$ shells is then the difference in the binding energies in these two calculations. Initially this was done with the *spsdpf* form of the Millener-Kurath interaction as described, e.g., in Ref. [49]. The final iterations were made with the *spsdpf* variant of the present PSDP interaction; the formation of this variant will be described in Sec. V D. The two results were in quite good agreement so that this final iteration was not really necessary. The correction factors just described are listed in Table IV. In general they are not large compared to $E^{(c)}_{\rm rms}$; however, this exercise had another aspect, namely, several levels for which the correction was unduly large were eliminated from the fit. A quantitative appraisal of the overall effect of this correction is that for the PSDP interaction $E^{(c)}_{\rm rms}$ increases from 373 keV with the correction to 392 keV without it.

C. Some aspects of the results

1. The 0p shell

The $0p$-shell interactions PWBP and PWBT obtained as part of simultaneous fits to the $0p$-shell and cross-shell data are compared to each other and to the PKUO interaction, and the P(5–16)T and P(10–16)T interactions in Table X. Recall that the PKUO interaction is the "bare G-matrix + core-polarization" interaction with the SPE tuned to the A=10–16 $0p$-shell data while the P(10–16)T interaction is the result of the "15 TBME + 2 SPE" fit to the A=10–16 $0p$-shell data.

2. The cross shell

The finally achieved $E^{(c)}_{\rm rms}$ values of 373 and 330 keV for the MD and MI-LC fits to the 165 cross-shell energies are extremely small compared to the A=5–16 $0p$-shell fits and to that obtained with the Millener-Kurath interaction. An appreciation of the main reason for the improvement in the MD fit can be had by reference to Table XI. In this table we show the results of fits similar

TABLE X. Comparison of the Kuo p-shell interaction, PKUO, to the four p-shell interactions obtained in the present study. The interactions are discussed in the text. The TBME of the P(5–16)T interaction have an A dependence of $(A/16)^{-0.20}$, the other four are independent of A.

$2j_1$	$2j_2$	$2j_3$	$2j_4$	J	T	Two-body matrix elements (MeV) PKUO	P(5–16)T	P(10–16)T	PWBP	PWBT
1	1	1	1	1	0	−2.5324	−3.9710	−4.0737	−3.4527	−3.4512
1	1	1	1	0	1	−0.0732	−1.3955	−1.2272	−1.1517	−1.2163
1	1	3	1	1	0	2.3142	1.7097	2.0672	1.6993	1.8096
1	1	3	3	1	0	1.7527	2.7889	2.0253	0.9227	0.6788
1	1	3	3	0	1	−3.9597	−3.1053	−3.5947	−3.7027	−3.8442
3	1	3	1	1	0	−7.2455	−6.0071	−5.7338	−6.9448	−6.8567
3	1	3	1	2	0	−6.5117	−4.7439	−4.2552	−3.9910	−3.9964
3	1	3	1	1	1	0.6427	1.0370	1.8179	1.8591	2.0492
3	1	3	1	2	1	−1.0768	−1.3248	−0.7945	−0.7463	−0.7818
3	1	3	3	1	0	5.0619	4.3951	4.4112	2.5273	2.4417
3	1	3	3	2	1	−1.8867	−1.7228	−1.4731	−1.7178	−1.6975
3	3	3	3	1	0	−2.4064	−1.8174	−2.1741	−3.8569	−4.1601
3	3	3	3	3	0	−5.6863	−6.2830	−6.4913	−6.0649	−6.0379
3	3	3	3	0	1	−3.3881	−4.1272	−4.0807	−3.9072	−3.8463
3	3	3	3	2	1	−0.8292	−1.1708	−1.0405	−0.7619	−0.7983
			$\Delta E_{\rm rms}$ =			1.312[a]	0.576	0.330	0.378	0.378
			$\epsilon_{3/2}$ =			1.128	2.460	1.765	1.548	1.678
			$\epsilon_{1/2}$ =			4.449	3.597	0.492	0.175	−0.121

[a] For a fit to 51 experimental energies with only the two SPE variable.

to the MD fit but with the $0p$-shell TBME fixed at either the PKUO or P(10–16)T values. The variables are the 2 $0p$-shell SPE plus either the four monopole variables or all ten potential variables designated in Table IX. The main lesson to learn from this table is the very significant improvement obtained by adding the monopole terms. The Millener-Kurath interaction is similar to the fourth row of the table. It has no monopole terms. Just including these brings the $E_{\rm rms}^{(\alpha)}$ within calling distance of our finally achieved $E_{\rm rms}^{(\alpha)}$. It is our feeling that the importance of the monopole terms lies in (1) better simulation of core polarization, and (2) more freedom in modeling the kinetic energy contributions.

We included very few $2\hbar\omega$ states in the fits. The ones included were all pure 2p-2h excitations in a *spsdpf* model space. How good are the predictions for other $2\hbar\omega$ states? Actually 48 other $2\hbar\omega$ states were monitored as this study progressed. These states are in nuclei from A=10 to 18 and have $E_{\rm rms}^{(2\hbar\omega)}$=669 keV for the PSDT interaction as compared to 330 keV for the 165 cross-shell levels included in the fit. If the 48 $2\hbar\omega$ states are also included in the fit then we obtain $E_{\rm rms}^{(p)}$=399 keV and $E_{\rm rms}^{(c)}$=407 keV. The same fit without the 48 states yielded the PSDT interaction with $E_{\rm rms}^{(p)}$=378 keV, $E_{\rm rms}^{(c)}$=330 keV. The large differences arises mainly from several very large deviations which are probably due at least partially to strong mixing between $0\hbar\omega$ and $2\hbar\omega$ states. If the five worst-fitting levels are eliminated then

TABLE XI. Root-mean-square deviations $E_{\rm rms}^{(\alpha)}$ (in keV) for some fits to a set of 201 energy levels [50 $0\hbar\omega$ p shell and 151 $1\hbar\omega$ and $2\hbar\omega$ cross shell]. The index α designates the total (t), p shell (p), and cross shell (c) values of $E_{\rm rms}^{(\alpha)}$. All datum were weighed equally. PKUO is the Kuo p-shell interaction and P(10–16)T is our adopted A=10–16 p-shell interaction — both described in Sec. III C. The $E_{\rm rms}^{(\alpha)}$ are only approximate since no iterations were performed.

Fit	Variables	$E_{\rm rms}^{(t)}$	$E_{\rm rms}^{(p)}$	$E_{\rm rms}^{(c)}$
PKUO + HKT(fixed)	2 SPE	2068	2393	1970
PKUO + HKT(fixed)	2 SPE + 4 central monopoles	856	1292	660
PKUO + HKT(variable)	2 SPE + 10 parameter potential	822	1295	598
P(10–16)T + H7B(fixed)	2 SPE	1918	2102	1873
P(10–16)T + H7B(fixed)	2 SPE + 4 central monopoles	492	355	533
P(10–16)T + H7B(variable)	2 SPE + 10 parameter potential	428	340	458

$E_{\rm rms}^{(2\hbar\omega)}$ drops from 669 keV to 495 keV. Also, no correction has been made for the omission of the $0s$ and $0f1p$ shells and, as will be shown in Sec. VI B, these corrections can be sizable.

D. Construction of the WBP and WBT interactions in a *spsdpf* model space

As we have made clear, there are many applications of the *psd* interactions for which it is desirable to include — in some manner or another — the effects of the $0s$ and $0f1p$ shells. Continuing the perturbative approach which guided us in the construction of our *psd* interactions, these effects are added by increasing the model space to include the $0s$ and $0f1p$ major shells. The total *sdfp* part of the interaction is taken to be the cross-shell WBMB interaction which has a proven ability to give a good representation of $A \approx 32$–44 nuclei [56]. The 768 TBME of this interaction are composed of the 63 $1s0d$ TBME of the W interaction — already included in the present cross-shell interactions — 510 cross-shell TBME connecting the $1s0d$ and $0f1p$ shells, and 195 $0f1p$ TBME. The reference nucleus for the $A^{-0.3}$ dependence of the WBMB TBME is ^{40}Ca, thus the WBMB TBME are multiplied by $(40/16)^{0.3}$ and given an A dependence of $(16/A)^{0.3}$. There remains the TBME involving the $0s$ shell and the TBME connecting the $0p$ shell with the $0f1p$ shell. These TBME are generated with the HKT potential and are assumed to be independent of A.

There are several ways to handle the $2\hbar\omega$ 1p-1h problem in an approximate manner. For the present applications we set all the $2\hbar\omega$ 1p-1h TBME connecting the $0s$ and $1s0d$ shells and the $0p$ and $0f1p$ shells equal to zero, thus guaranteeing that the Hartree-Fock condition be satisfied and allowing the removal of spurious center-of-mass motion [68]. We also add the forty $2\hbar\omega$ TBME connecting the $0p$ shell and $1s0d$ shells. These forty TBME are generated by the PSDP potential. They are needed for any attempts to calculate mixed $n\hbar\omega$ wave functions. The *spsdpf* interactions with the *psd* part from the PSDP and PSDT interactions are labeled WBP and WBT, respectively.

Now consider the single-particle energies. The SPE for the $0s$ shell was set to reproduce experimentally observed values [63]; more exactly, the $0s$-$0p$ interaction was adjusted so that the $0s$ binding energy varied linearly between -20.58 MeV at $A=4$ and -45.4 MeV at $A=16$. The spin-orbit splitting of the $0f$ and $1p$ shells is set at ^{41}Ca to be 6.5 and 1.8 MeV, respectively. These are the values used in the WBMB interaction for use in $A=32$–44 nuclei [56]. The SPE of the $0f_{7/2}$ and $1p_{3/2}$ orbits are then determined by a consideration of experimental spectroscopic results for ^{20}F which we now consider.

The known $1p_{3/2}$ spectroscopic strength S_n^+ in the ^{19}F$(d,p)^{20}$F reaction is concentrated in two states at 5936 and 6018 keV [35, 64, 65]. These two states also dominate the ^{19}F$(n,\gamma)^{20}$F thermal neutron capture. This (n,γ) result is interpreted as evidence for a direct $(l_n = 0, E1)$ capture mechanism for which the cross section is proportional to the l_n=1 S_n^+ value of the final state [65]. Both states have J^π=2$^-$ [65]. Our method for establishing the $1p_{3/2}$ SPE is to obtain the S_n^+ for the first 20 2$^-$ states as a function of the $1p_{3/2}$ SPE and to select that SPE value which best reproduces the experimental data. Our major criterion is that the summed spectroscopic strength in the energy region E_x=5.5–6.5 MeV approximately matches experiment. This procedure appears to be accurate to ~300 keV.

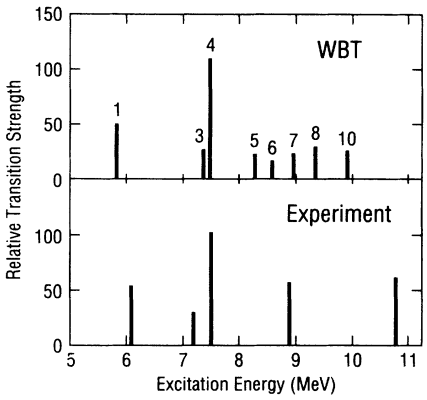

FIG. 2. Comparison of the experimental and predicted (WBT) distributions of 6$^-$ strength observed (Ref. [66]) in the ^{20}Ne$(p,n)^{20}$Na reaction. The experimental strengths are in arbitrary units. The predicted strengths of the $(6_k^-, 1)$ states are in units of $10^{-6}B(M6)$ and are labeled by the index k. Note the k=2 and 9 states are predicted to have negligible strength.

Recently, the J^π=6$^-$ strength in the ^{20}Ne$(p,n)^{20}$Na reaction was studied experimentally by Tamimi *et al.* [66]. This strength is determined by $1s0d \rightarrow 0f1p$ transitions and within the confines of a $0\hbar\omega + 1\hbar\omega$ model space, will proceed via the $0f_{7/2}$ component only. Thus the $0f_{7/2}$ SPE was determined by the best match of the 6$^-$ strength in a similar manner to the $1p_{3/2}$ determination. Comparison to experiment of the 6$^-$ strength distribution calculated with the finally chosen WBT interaction is made in Fig. 2.

The final single-particle binding energies at ^{16}O used in the WBT interaction are tabulated in Table XII.

TABLE XII. Final single-particle binding energies at ^{16}O used in the WBT interaction.

Orbit	SPE (MeV)
$0s_{1/2}$	−45.366
$0p_{3/2}$	−22.116
$0p_{1/2}$	−15.580
$0d_{5/2}$	−3.948
$0d_{3/2}$	1.647
$1s_{1/2}$	−3.164
$0f_{7/2}$	9.115
$0f_{5/2}$	13.458
$1p_{3/2}$	5.357
$1p_{1/2}$	5.851

VI. SOME ILLUSTRATIVE APPLICATIONS OF THE INTERACTIONS

A. The energy spectra of ^{20}F

The low-lying $0\hbar\omega$ and $1\hbar\omega$ spectra were calculated with the WBT interaction and are compared to experiment in Fig. 3. Note that WBP and WBT $0\hbar\omega$ spectra for $A>16$ default to that of the W interaction. There appear to be quite secure theoretical counterparts for all experimental levels below 2.4 MeV and all J^π assignments within this region are supported by the calculation, including the uncertain ones.

Between 2.5 and 4.0 MeV there appear to be 2 or 3 missing experimental levels. A 4^+ level corresponding to the 4_1^+ level predicted at 3666 keV has not been observed.

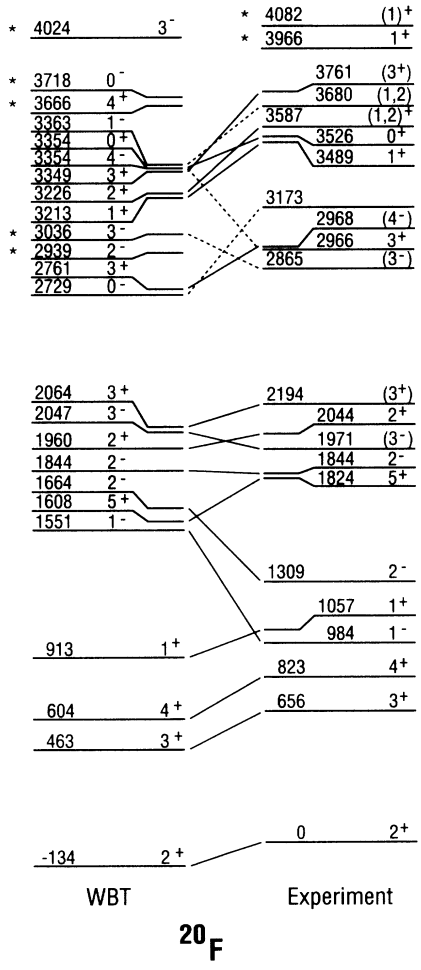

FIG. 3. The WBT predictions for the low-lying $T=1$ energy spectrum of ^{20}F. The levels are labeled by J^π and E_x (in keV). Experimentally uncertain J^π values are enclosed in parentheses. Experimental information is from Ref. [35]. Theoretical and experimental states are connected by solid lines if the correspondence between them seems certain and by dashed lines if it is speculative. Asterisks denote theoretical or experimental levels for which no correspondence is known.

There are only two experimental candidates for the 2_3^-, 3_2^-, and 4_1^- levels predicted at 2939, 3036, and 3354 keV. We have indicated one possible identification of the 3^- and 4^- states as those observed at 2865 and 2968 keV in which case the 2_3^- state is unobserved. It is also possible that the 2865- and 2968-keV levels are the 2_3^- and 3_2^- states, respectively, with the 4_1^- state unobserved.

We have tentatively identified the 0_1^- state with the experimental level at 3173 keV. There does not appear to be any strong evidence against this assignment although the 3173-keV level had been given a probable 1^+ assignment [35]. It was previously argued that if the 3173-keV level has $J^\pi=1^+$ then it is a $2\hbar\omega$ intruder [67]. The $2\hbar\omega$ spectrum is expected to commence with a predominantly $^{14}\mathrm{N}\otimes^{22}\mathrm{Ne}$ 1^+ state [67]. If not the 3173-keV level, then a strong candidate for the $2\hbar\omega$ 1_1^+ state is the 3966-keV level for which there is no $0\hbar\omega$ counterpart. (The $0\hbar\omega$ 1_3^+ state is predicted at 4792 keV.)

The $1\hbar\omega$ states of ^{20}F were not included in the least-squares fits. Assuming the identification shown for the eight $1\hbar\omega$ states in Fig. 3, the $E_{\mathrm{rms}}^{(c)}$ is 327 keV as opposed to 330 keV for the PSDT interaction. The twelve $0\hbar\omega$ states have $E_{\mathrm{rms}}^{(0\hbar\omega)}=231$ keV.

B. The energy spectra of ^{10}B and ^{10}Be

Our example of $A=10$ spectroscopy is an attempt to show how a well-tuned interaction can reveal deficiencies in the available experimental information and provide guidance for further experimental studies. The nuclei in question are ^{10}B and ^{10}Be. We have calculated the $T=0$ and 1 $0\hbar\omega$, $1\hbar\omega$, and $2\hbar\omega$ spectra of mass 10. We emphasize that the $0\hbar\omega$ and $2\hbar\omega$ spectra are unmixed. One motive for choosing this example was to illustrate the predictions for co-existing $0\hbar\omega$ and $2\hbar\omega$ states. The results are compared to experiment in Fig. 4, which is divided into three panels.

1. The even-parity $T=1$ states of ^{10}Be

We start a discussion of the results with the even-parity $T=1$ spectrum shown in the left panel. The experimental spectrum below 6 MeV is as expected; above 7 MeV it is largely unexplored. That is one experimental deficiency. Another centers on the wave function of the 7542-keV level. Is it the $0\hbar\omega$ 2_2^+ or the $2\hbar\omega$ 2_1^+ state, or a mixture of both? Where is the other 2^+ state? An obvious theoretical deficiency is the rather large discrepancy in E_x for the $2\hbar\omega$ 0_1^+ state. We might expect some improvement in this prediction when the mixing between $0\hbar\omega$ and $2\hbar\omega$ states is turned on. We find a similar discrepancy for the $2\hbar\omega$ $(0_1^+,1)$ state of ^{14}C. The overbinding of the $2\hbar\omega$ $(0_1^+,1)$ states in ^{10}B and ^{14}N is one of the more serious deficiencies in our interactions which we have found to date.

2. The even-parity $T=0$ states of ^{10}B

As for the $T=1$ spectrum just discussed, the experimental spectrum below ~6 MeV is as expected. The

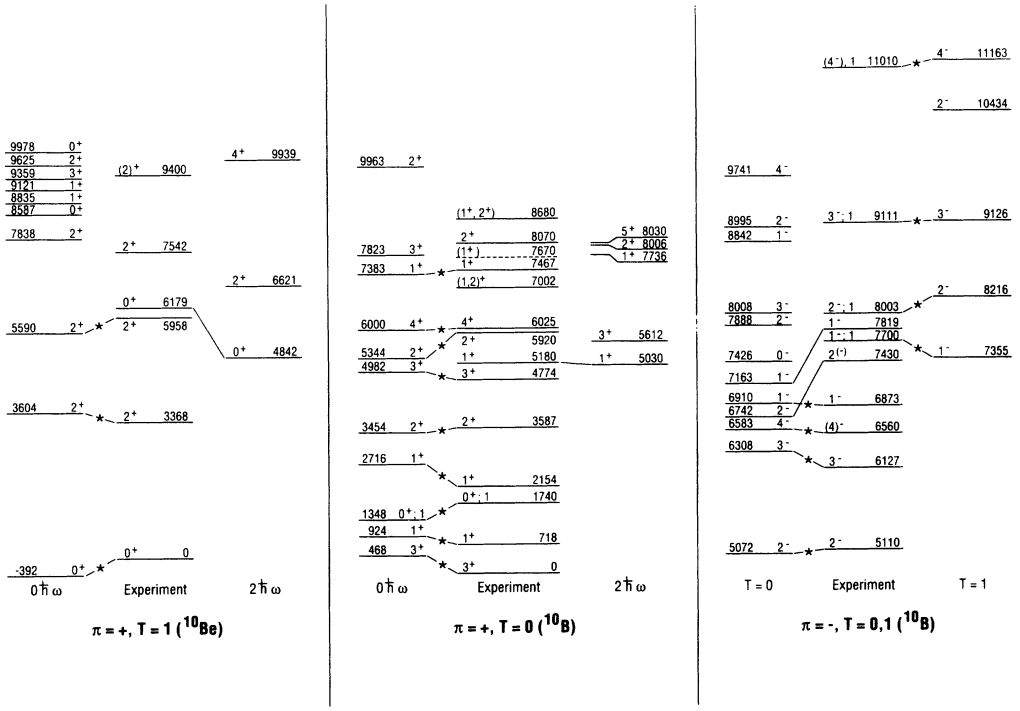

FIG. 4. Comparison of experimental and predicted (WBT) A=10 energy spectra. Levels are identified by J^π or J^π, T and by E_x in keV. Experimental information is from Ref. [35]. Experimentally uncertain J^π values are enclosed in parentheses. When the correspondence between an experimental level and a predicted level appears relatively certain they are connected by a solid line. Asterisks denote experimental levels included in the least-squares fits. The excitation energies for the T=1 odd-parity levels shown in the right panel are $E_x(^{10}\text{Be})$+1740 keV. In all three panels, all experimental and theoretical levels known below 10-MeV excitation are shown.

lowest $2\hbar\omega$ states have a large overlap with $^8\text{Be}(0^+)\otimes^{18}\text{F}$, hence the 1^+, 3^+, 5^+ sequence. A deficiency in the experimental data is that neither the 3^+ nor 5^+ levels have been observed. Also, it would be advantageous to have more experimental information bearing on the configurations of the states between 7 and 9 MeV. We note that there does not appear to have been any studies of multiparticle stripping to mass-10 nuclei. A good choice to study the $2\hbar\omega$ states would appear to be $^6\text{Li} + {}^7\text{Li}$ reactions leading to $^3\text{He} + {}^{10}\text{Be}$ and $^3\text{H} + {}^{10}\text{B}$.

We left $2\hbar\omega$ states with possible contributions from the $0s$ and $0f1p$ shells out of the *psd* fits because the correction due to this emission was expected to be relatively large and uncertain. As an example of its magnitude, the $2\hbar\omega$ $(1_1^+, 0)$ and $(0_1^+, 1)$ states are lowered by 995 and 807 keV, respectively, in going from the PSDT to WBT interactions. This binding increase is due in roughly 2:1 measure to the $0s$ and $0f1p$ shells. One reason for inclusion of the $0s$ and $0f1p$ shells is to allow the accurate removal of spurious center-of-mass motion from $2\hbar\omega$ states in $A \leq 16$ nuclei. The ^{10}B $2\hbar\omega$ states calculated with the PSDT interaction have some spuriosity and its removal in going to the WBT interaction will decrease the magnitude of the binding energies. The fact that the WBT interaction binds the ^{10}B states more than the PSDT interaction means that allowed types of $2\hbar\omega$ excitations are dominating the spurious ones. Since we have turned off the 1p-1h $2\hbar\omega$ TBME, these excitations are "sequential" $\Delta\mathcal{N}$=1 transitions, i.e., $0s \rightarrow 0p \rightarrow 1s0d$ and $0p \rightarrow 1s0d \rightarrow 0f1p$.

3. *Odd-parity states of* ^{10}B

Our predictions are compared to the known experimental levels in the right panel of Fig. 4. The agreement between experiment and the WBT predictions is satisfactory. There are good theoretical counterparts for the only two experimentally known odd-parity levels not included in the fits (although the predictions are significantly too overbound). The experimental information is once-again deficient in that there are no known odd-parity T=0 levels above 8 MeV. One other A=10 $1\hbar\omega$ state is known, namely the $(2^-, 2)$ state (No. 9 of Table IV) which we predict to be the ^{10}Li ground state. If this prediction is true, this is a second case of a $0p$-shell nucleus with a $1\hbar\omega$ ground state — ^{11}Be being the first one.

C. Binding energies of exotic neutron-rich nuclei

1. *Coulomb energies of exotic nuclei*

For most of the states listed in Table XIII the positions of the analogues of the nuclei with $T_z = T$ in the $T_{z_{\min}}$ nuclei are not known and it is necessary to rely on the differences of Coulomb energies in order to obtain the values

TABLE XIII. Exotic $T_z = T$ neutron-rich nuclei and their analogues in the $T_{z_{\min}}$ nuclei. All states shown are included in the cross-shell fits. ^{11}Li (No. 1) is from Table III. ^{13}Be, ^{14}B, and the N isotopes (Nos. 2,4,13–16) are from Table IV, and the remainder are from Table VI. $E_{B_{\rm exp}}$ is the experimental binding energy from Ref. [70]. $\Delta = E_{B_{\rm corr}} - E_{B_{\rm exp}}$.

No.	$T_z = T$ Nucleus	$T_z = T_{z_{\min}}$ Nucleus	$2J^\pi$	$2T$	$E_{B_{\rm exp}}$ (MeV)	$\Delta E_{B_{\rm exp}}$	$E_{B_{\rm corr}}$ (MeV)	Δ (MeV)
1	^{11}Li	^{11}B	3^-	5	−45.589	80	−45.733	0.144
2	^{13}Be	^{13}C	1^+	5	−66.802	500	−67.218	0.416
3	^{14}Be	^{14}N	0^+	6	−69.986	108	−69.840	−0.146
4	^{14}B	^{14}N	4^-	4	−85.424	21	−85.409	−0.015
5	^{15}B	^{15}N	3^-	5	−88.188	22	−88.452	0.264
6	^{17}B	^{17}O	3^-	7	−89.586	36	−89.976	0.390
7	^{19}B	^{19}F	3^-	9	$\leq$ −89.586[a]		−89.096	−0.490
8	^{17}C	^{17}O	3^+	5	−111.479	17	−111.426	−0.053
9	^{18}C	^{18}F	0^+	6	−115.663	30	−116.134	0.471
10	^{19}C	^{19}F	1^+	7	−115.829	108	−115.242	−0.587
11	^{20}C	^{20}Ne	0^+	8	−119.174	201	−119.261	0.087
12	^{22}C	^{22}Na	0^+	10	$\leq$ −119.174[a]		−119.041	−0.133
13	^{19}N	^{19}F	1^+	5	−132.017	16	−132.323	0.306
14	^{20}N	^{20}Ne	0^+	6	−134.185	52	−134.235	0.050
15	^{21}N	^{21}Ne	1^-	7	−138.790	89	−138.915	0.125
16	^{22}N	^{22}Ne	0^+	8	−140.013	196	−140.317	0.304

[a] The limits for ^{19}B and ^{22}C correspond to $S(2n)$=0 and arise because these bodies are stable against this decay mode.

of E_x used in the fits and listed in the table. The general behavior of Coulomb displacement energies in light nuclei is well documented for $T \leq 2$ and is not very sensitive to T, especially for $T > 1$. When the analogue state is not known, we use the empirical relationship [69]

$$\Delta E_c(A, Z-1) \equiv E_c(A, Z) - E_c(A, Z-1) = 1444\bar{Z}/A^{1/3} - 1022 \text{ keV} \quad (6)$$

where $\bar{Z}$ is the average of $Z-1$ and Z. Equation (6) gives a quite good account of the Z and A dependence of $\Delta E_c(A, Z)$ for $T > 1$.

The E_x [in the $(A, T_{z_{\min}})$ nucleus] for the analogues of the neutron-rich nuclei listed in the first column of Table XIII are obtained from consecutive applications of the relation

$$E_x(A, T_z) = E_x(A, T_z+1) + Q_\beta(A, T_z+1) + \Delta E_c(A, T_z+1) - 782 \text{ keV} \quad (7)$$

with all energies in keV and ΔE_c obtained from Eq. (6). To predict the mass of the T_z state from a predicted value for $E_x(A, T_{z_{\min}})$ or $E_{B_{\rm corr}}(A, T_{z_{\min}})$, the procedure is reversed.

The listed experimental binding energies $E_{B_{\rm exp}}$ are from the 1988 mass table or its 1990 midstream update [70]. All E_x values are obtained using Eqs. (6, 7) except that for ^{14}B which is based on the $(2^-, 2)$ state at 22100-keV excitation in ^{14}C [35]. The limit for the $E_{B_{\rm exp}}$ and E_x of ^{19}B is based on the observation that it is stable against two-neutron emission [71].

2. *Binding energies and neutron separation energies of boron isotopes*

We choose the A=14–20 B isotopes to exemplify the application of the PSDT interaction to the prediction of neutron-rich masses. The low-lying np-3h spectra of A=15–20 boron isotopes are shown in Fig. 5 and the relevant mass data are collected in Table XIV. The separation energies are simply

$$S(n) = E_B(A, T_z) - E_B(A-1, T_z - \tfrac{1}{2}), \quad (8)$$

$$S(2n) = E_B(A, T_z) - E_B(A-2, T_z - 1) \quad (9)$$

where E_B stands for either the experimental or predicted binding energies.

The predicted masses are in satisfactory agreement with the experimental ones when the latter are known. ^{16,18}B are predicted to be unstable against neutron emission, in agreement with experiment [35]. Our one failure is that we predict ^{19}B to be unstable to two-neutron emission by 875 keV when, in actual fact, it is known to be stable against all particle emission [71]. However, reference to the deviation between experiment and theory which is shown in Tables IV and V, shows that a disagreement of this amount is not too unusual especially since part of the disagreement arises because ^{17}B is predicted to be 390 keV more bound than experiment.

D. The β^- decay of ^{16}C

The $2\hbar\omega$ T=1 states of ^{16}O (and thus ^{16}N) can contain ΔQ=2 1p-1h excitations of the ^{16}O core. Thus they were not included in the least-squares fit. However, the T=2

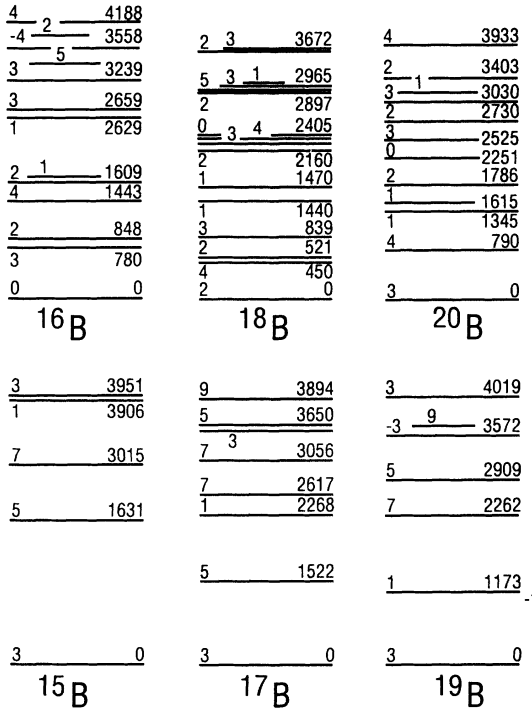

FIG. 5. The PSDP predictions for the low-lying $(\pi 0p)^{-3}(\nu 1s0d)^{A-13}$ spectra for A=15–20 boron isotopes. The even-A and odd-A levels are labeled by J and $2J$, respectively, and by E_x (in keV). All have odd parity.

states contain no such admixtures and so Gamow-Teller matrix elements for ^{16}C$(\beta^-)^{16}$N(1^+) transitions are expected to be insensitive to the 1p-1h admixtures in the 1^+ states. This expectation will be tested.

It has been known since the original study of the decay of ^{16}C by Alburger and Wilkinson [72] that the Millener-Kurath interaction fails to explain the observed Gamow-Teller decay to the $(1_1^+,1)$ and $(1_2^+,1)$ states at 3353 and 4320 keV. Experimentally the decay to these two states have Gamow-Teller transition probabilities B(GT) of 1.728±0.040 and 0.917±0.100, where B(GT) is dimensionless and for a pure Gamow-Teller decay is defined by

$$B(\mathrm{GT}) = 6139/ft. \tag{10}$$

In Eq. (10) f is the Fermi integral for Gamow-Teller decays and t is the partial half-life (in s) for the branch in question. As quoted in Ref. [72], Millener obtained B(GT)=0.002 and 1.413 for these two branches. A later calculation with somewhat different SPE parameters yielded 0.002 and 0.567 [74]. Both of these calculations used the MK interaction and a Gamow-Teller operator appropriate for free nucleons. The failure to explain the branch to the $(1_1^+,1)$ state is dramatic.

We have calculated the Gamow-Teller decay of ^{16}C with the PSDP, PSDT, and WBT interactions. The results are given in Table XV where the predicted transition probability is shown for the k=1–5 $2\hbar\omega$ $(1_k^+,1)$ model states of ^{16}N. The transition probability was calculated with effective operators derived from experimental data. For $(1s0d) \rightarrow (1s0d)$ transitions we use the results of Brown and Wildenthal [9]; while effective values for the three $0p$-shell transitions are obtained from a least-squares fit [75] to experimental Gamow-Teller matrix elements connecting states describable by the P(10–16)T interaction. As an example of the effect of these empirical operators, the WBT B(GT) for the first two transitions of Table XV are quenched by a factor of 0.57.

First consider the E_x of Table XV. There is considerable uncertainty as to the identity of the k=3–5 1^+ levels of ^{16}N. As regards the k=3 state, Ajzenberg-Selove identifies the J=0 or 1 (unknown parity) 5318-keV state observed by Fortune and Silverman [76] in the ^{10}B(^{7}Li,p)^{16}N reaction with the 1^+ anomaly at 5.24 MeV invoked (but not directly observed) by Zeitnitz *et al.* [77] to explain their ^{15}N(n,n') results. However, this identification is in contradiction with the reported widths of the states in the two reactions. We regard the placement of the third 1^+ state as uncertain and arbitrarily assume that it is the analogue of the $(1_3^+,1)$ state identified at 18.79 MeV in ^{16}O in the (p,γ) study of Snover, Ikossi, and Trainor [78]. The k=4 and 5 1^+ states of Table XV are from Ref. [35].

We show the results for three interactions in Table XV to illustrate several points. First, the sensitivity of the E_x and B(GT) to the *psd* interaction is seen by compar-

TABLE XIV. Mass and neutron separation energy predictions for the A=13–20 boron isotopes. The listed $S(n)$ and $S(2n)$ are predictions. Allowed neutron decays have positive separation energies. The limits for ^{19}B are associated with $S(2n)$=0.0 keV and arise because it is observed to be stable. $\Delta = E_{B_{\mathrm{corr}}} - E_{B_{\mathrm{exp}}}$.

A	$E_{B_{\mathrm{exp}}}$ (keV) Expt.	$E_{B_{\mathrm{corr}}}$ (keV) Theory	Δ (keV)	$S(n)$ (keV)	$S(2n)$ (keV)
13	−84454	−84423	−31		
14	−85424	−85409	−15	−986	
15	−88188	−88452	264	−3043	−4029
16		−88288		164	−2879
17	−89586	−89976	390	−1688	−1524
18		−88101		1875	187
19	≤ −89586	−89101	≤ −490	−1000	875
20		−86163		−2938	−1938

TABLE XV. Comparison of predicted and experimental (Expt.) B(GT) values for the decay of ^{16}C to the k=1–5 $(1_k^+, 1)$ states of ^{14}N.

k	E_x (keV)				B(GT)			
	Expt.	PSDP	PSDT	WBT	Expt.	PSDP	PSDT	WBT
1	3353	2858	2881	2835	1.728	0.813	1.231	1.316
2	4320	3325	3612	3470	0.917	0.621	0.415	0.321
3	(5894)[a]	5559	5638	5474	< 1.3[b]	1.053	1.069	0.560
4	(6505)[a]	6317	6443	6136		0.020	0.001	0.541
5	(7020)[a]	6884	6997	6273		1.352	1.550	0.409

[a] Speculative; see text.

[b] The limit corresponds to a branching ratio limit of $\leq$2.0% [73]. The detection efficiency for the β-delayed neutrons in the experimental study of Ref. [72] falls off quite rapidly with energy. Thus no useful limits were set on decays to the k=4 and 5 states listed above.

ing the PSDP and PSDT results. The E_x are relatively insensitive and the B(GT) relatively sensitive to the *psd* interaction. Second, the comparison of the PSDT and WBT results reveals interesting features. The lowest two ^{16}N 1^+ states contain small ΔQ=2 components; i.e., they are insensitive to the expansion of the model space to include the $0s$ and $0f1p$ shells. However, as the excitation energy increases, the effect on both the E_x and B(GT) is considerable. We will remark further on this comparison in the conclusions of Sec. VII.

Comparing experiment to the preferred result of Table XV — that of the WBT interaction — it is seen that the bulk of the disagreement noted for the Millener-Kurath interaction has been corrected. From a consideration of the sensitivity to the interaction and also to the effective operators, it is concluded that the disagreement that remains is not serious, i.e., is within the overall uncertainty in the modeling.

VII. CONCLUSIONS

Shell-model interactions encompassing the first four oscillator shells have been constructed for use with unmixed $n\hbar\omega$ calculations in $A \approx$10–22 nuclei. The final form was arrived at after exhaustive tests of many alternatives. We believe it represents a near optimization of the desired combination of simplicity and accuracy. Two assumptions are basic to our approach. First, the $1s0d$-shell part of the *psd* interaction is not changed appreciably from the W interaction which was determined by considering $1s0d$ states alone. In contrast, The $0p$-shell part of the *psd* interaction was determined simultaneously with the cross-shell part and, as can be seen by reference to Table X, there are some large differences between the p-shell interactions obtained from the p-shell alone — P(10–16)T and P(5–16)T — and those resulting from simultaneous p-shell and cross-shell fits — PWBP and PWBT. This suggests two areas of future study: (1) Would an appreciable better fit result if the $1s0d$-shell interaction were also varied? (2) What are the reasons and consequences of the changes in the p-shell interaction? It is interesting to note one consequence; namely, the large changes in three of the p-shell TBME involving the $0p_{3/2}$ orbit appear to be the major cause for the great improvement in agreement with the experimental ^{16}C Gamow-Teller decays.

Our second basic assumption — closely related to the first one — is that the influence of other shells can be added perturbatively. Thus the model space was expanded by including TBME and SPE which were not directly part of the fitted interaction. Enough tests of this procedure have been made to show it is adequate for most low-lying states in the A=10–22 region but that a more quantitative determination of this part of the interaction should be made in order to study states with large contributions from these shells. This is a further area of future study which should be pursued.

A crucial procedure in our approach is to describe each major shell and each cross-shell interaction as a separate entity. Thus, in principle, we envisage the total interaction describing the first four oscillator shells as seven separate interactions. We have dealt with states which depend primarily on three of these seven interactions and aimed at a determination of these three by least-squares fitting to binding energies. Fortunately, the $1s0d$ part of the interaction was previously determined in a way which matched our approach. Thus we concentrated on joining the $0p$ and *psd* parts of the interaction to the $1s0d$ part. A second crucial ingredient in our approach is that no mixing of $n\hbar\omega$ and $(n+2)\hbar\omega$ states is attempted. We feel that such mixing will have serious flaws unless the two problems associated with this mixing are addressed to a sufficient degree of accuracy. These problems are the violation of the Hartree-Fock condition [57, 79] and the problems associated with the truncation of the n=0,2,4,... series at n=2 [56, 79, 80]. Incorporation of such mixing in a satisfactory way is yet another area for future study.

The procedures described in the last paragraph are hardly controversial and it is not surprising that they work. They are dealt on here because they emphasize the difference of our approach and that of the Utrecht group which has provided most of the activity in this field in the last few years. The basic premises of the Utrecht approach is that one interaction can describe states in several major shells and that the interaction is in a translationally-invariant oscillator basis. The var-

ious studies [22–27] using this assumption comprise an admirable and informative attempt to describe the states in a conceptually simple manner. This approach works well enough for a small model space. Thus, the van Hees-Glaudemans [22, 23] $(0+1)\hbar\omega$ interaction for $A \leq 16$ nuclei provides useful wave functions for the calculation of nuclear observables. However when expanded to include parts of the first four major shells [26, 27], $E_{\rm rms}$ becomes quite large and the wave functions develop serious flaws [79]. Finally, the attempt to provide an interaction to describe mixed $(0+2)\hbar\omega$ states ran afoul of the two problems mentioned in the previous paragraph [79] as well as the deficiencies associated with the description of four major shells with a single interaction.

We have given some examples of the application of the interactions developed here. Planned future studies include (1) comprehensive calculations of Gamow-Teller and first-forbidden beta-decay observables, (2) binding energy predictions for exotic neutron-rich nuclei, (3) consideration of $(0+2+4)\hbar\omega$ states, and (4) calculation of parity non-conservation matrix elements for A=16–21.

ACKNOWLEDGMENTS

Research was supported in part by the U.S. Department of Energy under Contracts Nos. DE-AC02-76CH00016 with Brookhaven National Laboratory and in part by the National Science Foundation under Grant No. PHY-90-17077 with Michigan State University. D. J. Millener is to be thanked for countless consultations, for sharing his considerable knowledge of the experimental levels involved here, and for providing the linear combination part of the least-squares fitting routine.

[1] S. Cohen and D. Kurath, Nucl. Phys. **73**, 1 (1965).
[2] B. M. Preedom and B. H. Wildenthal, Phys. Rev. C **6**, 1633 (1972).
[3] W. Chung, Ph.D. thesis, Michigan State University, 1976.
[4] B. H. Wildenthal, Prog. Part. Nucl. Phys. **11**, 5 (1984).
[5] B. A. Brown, W. A. Richter, R. E. Julies, and B. H. Wildenthal, Ann. Phys. (N.Y.) **182**, 191 (1988).
[6] B. A. Brown and B. H. Wildenthal, Annu. Rev. Nucl. Part. Sci. **38**, 29 (1988).
[7] R. E. Julies, W. A. Richter, and B. A. Brown (unpublished).
[8] P. J. Brussard and P. W. M. Glaudemans, *Shell-Model Applications in Nuclear Spectroscopy* (North-Holland, Amsterdam, 1977).
[9] B. A. Brown and B. H. Wildenthal, At. Data Nucl. Data Tables **33**, 347 (1985).
[10] T. T. S. Kuo and G. E. Brown, Nucl. Phys. **85**, 40 (1966).
[11] T. T. S. Kuo, Nucl. Phys. **A103**, 71 (1967); J. Shurpin, T. T. S. Kuo, and D. Strottman, *ibid.* **A408**, 310 (1983).
[12] W. A. Richter, M. G. Van der Merwe, R. E. Julies, and B. A. Brown, Nucl. Phys. **A523**, 325 (1991).
[13] J. P. Elliott and B. H. Flowers, Proc. R. Soc. London, Ser. A **242**, 57 (1957).
[14] E. C. Halbert and J. B. French, Phys Rev. **105**, 1563 (1957).
[15] D. J. Millener and D. Kurath, Nucl. Phys. **A255**, 315 (1975).
[16] I. Talmi and I. Unna, Annu. Rev. Nucl. Sci. **10**, 353 (1960).
[17] P. J. Ellis and T. Engeland, Nucl. Phys. **A144**, 161 (1970).
[18] T. Engeland and P. J. Ellis, Nucl. Phys. **A181**, 368 (1972).
[19] S. Lie, T. Engeland, and G. Dahll, Nucl. Phys. **A156**, 449 (1970).
[20] S. Lie and T. Engeland, Nucl. Phys. **A169**, 617 (1971).
[21] S. Lie, Nucl. Phys. **A181**, 517 (1972).
[22] A. G. M. van Hees, Ph.D. thesis, University of Utrecht, 1982.
[23] A. G. M. van Hees and P. W. M. Glaudemans, Z. Phys. A **314**, 314 (1983); **315**, 223 (1984).
[24] A. A. Wolters, Ph.D. thesis, University of Utrecht, 1989.
[25] A. A. Wolters, A. G. M. van Hees, and P. W. M. Glaudemans, Phys. Rev. C **42**, 2053 (1990); 2062 (1990).
[26] N. A. F. M. Poppelier, L. D. Wood, and P. W. M. Glaudemans, Phys. Lett. **157B**, 120 (1985).
[27] N. A. F. M. Poppelier, Ph.D. Thesis, University of Utrecht, 1989.
[28] B. A. Brown, A. Etchegoyen, W. D. M. Rae, and N. S. Godwin (unpublished).
[29] D. H. Glockner and R. D. Lawson, Phys. Lett. **53B**, 313 (1974).
[30] E. K. Warburton, J. A. Becker, B. A. Brown, and D. J. Millener, Ann. Phys. (N.Y.) **187**, 471 (1988).
[31] E. G. Adelberger and W. C. Haxton, Annu. Rev. Nucl. Sci. **35**, 501 (1985).
[32] B. A. Brown, W. A. Richter, and N. S. Godwin, Phys. Rev. Lett. **45**, 1681 (1980).
[33] A. Hosaka, K.-I. Kubo, and H. Toki, Nucl. Phys. **A244**, 76 (1985).
[34] A comprehensive report of results of the W interaction (Ref. [4]) has not yet been published. However, a summary of binding energies for A=17–39 nuclei has been privately circulated. A description of the method used to calculate the Coulomb contribution to the experimental binding energy is given in Ref. [3].
[35] F. Ajzenberg-Selove, Nucl. Phys. **A490**, 1 (1988); **A506**, 1 (1990); **A523**, 1 (1991); **A460**, 1 (1986); **A475**, 1 (1987).
[36] D. J. Millener, D. I. Sober, H. Crannell, J. T. O'Brien, L. W. Fagg, S. Kowalski, C. F. Williamson, and L. Lapikás, Phys. Rev. C **39**, 14 (1989).
[37] S. S. Saha, W. W. Daehnick, S. A. Dytman, P. C. Li, J. C. Hardie, G. P. A. Berg, C. C. Foster, W. P. Jones, D. W. Miller, and E. J. Stephenson, Phys. Rev. C **40**, 39 (1989).
[38] E. K. Warburton and W. T. Pinkston, Phys. Rev. **118**, 733 (1960).
[39] C. C. Maples, Ph.D. thesis, University of California Report No. LBL-253, 1971; C. C. Maples and J. Cerney, Phys. Lett. **38B**, 504 (1972); D. G. Fleming, J. Cerney, C. C. Maples, and N. Glendenning, Phys. Rev. **166**, 1012 (1968).
[40] W. W. True and E. K. Warburton, Nucl. Phys. **22**, 426 (1961).
[41] D. J. Millener, private communication.
[42] E. Korkmaz *et al.*, Phys. Rev. C **40**, 813 (1989).
[43] D. E. Alburger and D. J. Millener, Phys. Rev. C **20**, 1891 (1979).
[44] C. E. Hyde-White *et al.*, Phys. Rev. C **35**, 880 (1987).

[45] S. S. Saha, W. W. Daehnick, S. A. Dytman, P. C. Li, J. C. Hardie, G. P. A. Berg, C. C. Foster, W. P. Jones, D. W. Miller, and E. J. Stephenson, Phys. Rev. C **42**, 922 (1990).
[46] C. L. Blilie *et al.*, Phys. Rev. C **30**, 1989 (1984).
[47] D. M. Manley *et al.*, Phys. Rev. C **36**, 1700 (1987).
[48] S. M. Aziz, Ph.D. thesis, Indiana University, 1988.
[49] E. K. Warburton and D. J. Millener, Phys. Rev. C **39**, 1120 (1989).
[50] D. M. Manley *et al.*, Phys. Rev. C **43**, 2147 (1991).
[51] L. M. Martz, Ph.D. thesis, Yale University, 1978.
[52] D. J. Millener, Workshop on Bound and Continuum Aspects of the Structure of Light Nuclei, Lawrence Livermore National Laboratory, 1989 (unpublished). An abstract of this enlightening presentation of selective problems in the structure of light nuclei is available from D.J.M.
[53] D. J. Millener, private communication.
[54] D. J. Millener, Phys. Rev. C **36**, 1643 (1987).
[55] P. Goldhammer, J. R. Hill, and J. Nachamkin, Nucl. Phys. **A106**, 62 (1968).
[56] E. K. Warburton, J. A. Becker, and B. A. Brown, Phys. Rev. C **41**, 1147 (1990).
[57] T. Hoshino, H. Sagawa, and A. Arima, Nucl. Phys. **A481**, 458 (1988).
[58] T. T. S. Kuo, private communication.
[59] G. Bertsch, J. Borysowicz, H. McManus, and W. G. Love, Nucl. Phys. **A284**, 399 (1977).
[60] A more exact description of the M3Y potential used here and the origin of its acronym is given in footnote 13 of Ref. [61].
[61] E. K. Warburton and B. A. Brown, Phys. Rev. C **43**, 602 (1991).
[62] M. Lacombe, B. Loiseau, J. M. Richard, R. Vinh Mau, J. Côté, P. Pirés, and R. de Tourreil, Phys. Rev. C **21**, 861 (1980).
[63] K. Bear and P. E. Hodgson, J. Phys. G **4**, L287 (1978).
[64] C. A. Mosley and H. T. Fortune, Phys. Rev. C **16**, 1697 (1977).
[65] S. Raman, private communication.
[66] N. Tamimi, B. D. Anderson, A. R. Baldwin, T. Chittrakarn, M. Elaasar, R. Madey, D. M. Manley, M. Mostajabodda'vati, J. W. Watson, W.-M. Zhang, J. A. Carr, and C. C. Foster, Phys. Rev. C **45**, 1005 (1992).
[67] D. E. Alburger, G. Wang, and E. K. Warburton, Phys. Rev. C **35**, 1479 (1987).
[68] For exact removal of spuriosity the next major shell — $0g1d2s$ — must be added for $2\hbar\omega$ excitations of states with active $1s0d$ nucleons. By comparison of results with and without this shell, we find its omission causes negligible error for the low-lying $2\hbar\omega$ states of $A < 20$ nuclei.
[69] M. S. Antony, J. Britz, J. B. Bueb, and A. Pape, At. Data Nucl. Data Tables **33**, 447 (1985).
[70] A. H. Wapstra, G. Audi, and R. Hoekstra, At. Data Nucl. Data Tables **39**, 281 (1988); midstream update of the mass table, private communication from G. Audi.
[71] J. A. Musser and J. D. Stevenson, Phys. Rev. Lett. **53**, 2544 (1984).
[72] D. E. Alburger and D. H. Wilkinson, Phys. Rev. C **13**, 835 (1976).
[73] D. E. Alburger, private communication.
[74] K. A. Snover, E. G. Adelberger, P. G. Ikossi, and B. A. Brown, Phys. Rev. C **27**, 1837 (1983).
[75] W.-T. Chou, E. K. Warburton, and B. A. Brown (unpublished).
[76] H. T. Fortune and B. H. Silverman, Phys. Rev. C **29**, 1761 (1984).
[77] B. Zeitnitz *et al.*, Nucl. Phys. **A166**, 443 (1971).
[78] K. A. Snover, P. G. Igossi, and T. A. Trainor, Phys. Rev. Lett. **43**, 117 (1979).
[79] D. J. Millener, A. C. Hayes, and D. D. Strottman, Phys. Rev. C **45**, 473 (1992).
[80] P. J. Ellis and L. Zamick, Ann. Phys. (N.Y.) **55**, 61 (1969).